



# RECFA meeting



## Astroparticle physics in Slovakia

*Pavol Bobik*

*Institute of Experimental Physics*

*Slovak Academy of Sciences*

# Astroparticle physics in Slovakia

## 1. Cosmic rays models selected results

- *Models of cosmic rays propagation - modulation in heliosphere*

## 2. Ground measurements selected results

- *Measurements at Lomnicky stit observatory*

## 3. Particle space experiments in preparation

## 4. EUSO missions

*Not in any way complete overview of astroparticle physics in Slovakia, only selected results from last years are presented.*

# Propagation of Cosmic rays in the Heliosphere

## Parker transport equation

Propagation in the heliosphere is described by Parker (1965) equation:

$$\frac{\partial U}{\partial t} = \nabla \cdot (\underbrace{\mathbf{K}^S \cdot \nabla U}_{\text{Diffusion}} - \underbrace{\mathbf{V}_{\text{sw}} U}_{\text{Convection}} - \underbrace{\langle \mathbf{v}_D \rangle U}_{\text{Drift}}) + \underbrace{\frac{1}{3} (\nabla \cdot \mathbf{V}_{\text{sw}}) \frac{\partial}{\partial T} (\alpha T U)}_{\text{Energetic Loss}}$$

$U$  is Cosmic Rays number density per unit interval of kinetic energy

### Diffusion

Small Scale  
magnetic Field  
irregularity

### Convection

Solar wind  
moving out  
from the Sun

### Drift

Large scale  
magnetic field  
structure

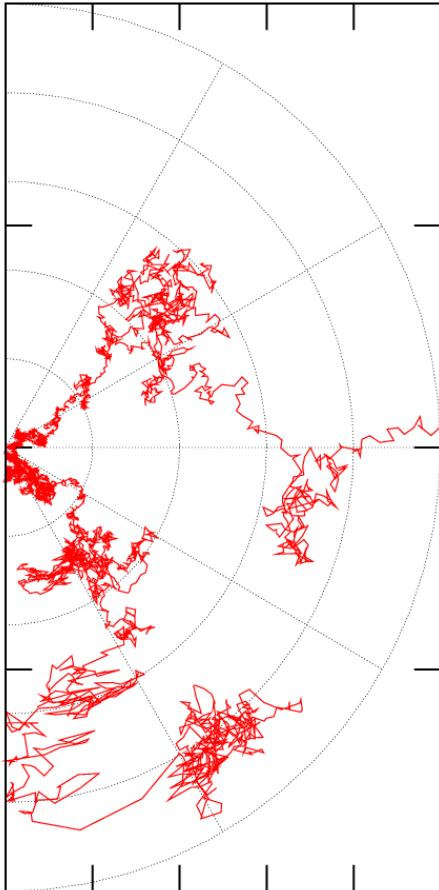
### Energetic Loss

Due to adiabatic  
expansion of the  
solar wind

Propagation of CR in the heliosphere is described  
by Parker (1965) equation:

$$\frac{\partial U}{\partial t} = \nabla \cdot (\mathbf{K}^S \cdot \nabla U - \mathbf{V}_{\text{sw}} U - \langle \mathbf{v}_D \rangle U) + \frac{1}{3} (\nabla \cdot \mathbf{V}_{\text{sw}}) \frac{\partial}{\partial T} (\alpha T U)$$

A Monte Carlo Approach - *Ito's lemma*, see e.g. Gardiner, 1985  
The 2D **Heliosphere Modulation** Monte Carlo Code: **HelMod**



*Stochastic Differential Equations (SDE)*

$$\begin{aligned} dr &= \frac{1}{r^2} \frac{\partial}{\partial r} (r^2 K_{rr}) dt - \frac{\partial}{\partial \mu} \left( \frac{K_{r\mu} \sqrt{1 - \mu^2}}{r} \right) dt + (V_{\text{sw}} + v_{dr}) dt + (2K_{rr})^{1/2} R_r \sqrt{dt} \\ d\mu &= -\frac{1}{r^2} \frac{\partial}{\partial r} (r K_{\mu r} \sqrt{1 - \mu^2}) dt + \frac{\partial}{\partial \mu} \left( K_{\mu\mu} \frac{1 - \mu^2}{r^2} \right) dt - \frac{1}{r} v_{d\mu} \sqrt{1 - \mu^2} dt \\ &\quad + \frac{-2K_{r\mu}}{r} \left( \frac{1 - \mu^2}{2K_{rr}} \right)^{1/2} R_r \sqrt{dt} + \frac{1}{r} \left( (1 - \mu^2) \frac{K_{\mu\mu} K_{rr} - K_{r\mu}^2}{0.5K_{rr}} \right)^{1/2} R_\mu \sqrt{dt} \\ dT &= -\frac{\alpha_{\text{rel}} T}{3r^2} \frac{\partial V_{\text{sw}} r^2}{\partial r} dt \end{aligned}$$

2-Dimensional set of SDEs

Details of HelMod modulation code, and how to compute the SDE,  
could be found in [Bobik et al. Ap.J. 2012, 745:132]



# HelMod – selected results

error-weighted  
root mean square of  
the relative difference  
between experimental data  
and those resulting from  
simulated differential  
intensities

$$\eta_{\text{rms}} = \sqrt{\frac{\sum_i (\eta_i / \sigma_{\eta,i})^2}{\sum_i 1 / \sigma_{\eta,i}^2}}$$

$$\eta_i = \frac{f_{\text{sim}}(T_i) - f_{\text{exp}}(T_i)}{f_{\text{exp}}(T_i)}$$

Observations	“L” Model	“R” Model
BESS–1999	8.7	8.0
BESS–2000	16.2	15.8
BESS–2002	12.7	15.0

---

Observations	“L” Model	“R” Model
BESS–1997	9.2	17.7
AMS–1998	4.6	7.9
BESS–1998	9.1	14.1
PAMELA–2006/08	7.1	13.4

Table 2 and 4

## Systematic Investigation of Solar Modulation of Galactic Protons for Solar Cycle 23 using a Monte Carlo Approach with Particle Drift Effects and Latitudinal Dependence

P. Bobik<sup>1</sup>, G. Boella<sup>2,3</sup>, M.J. Boschini<sup>2,4</sup>, C. Consolandi<sup>2</sup>, S. Della Torre<sup>2,5</sup>, M. Gervasi<sup>2,3</sup>, D. Grandi<sup>2</sup>, K. Kudela<sup>1</sup>, S. Pensotti<sup>2,3</sup>, P.G. Rancoita<sup>2</sup> and M. Tacconi<sup>2</sup>

*Istituto Nazionale di Fisica Nucleare, INFN, Milano-Bicocca, Milano (Italy), I20126*

piergiorgio.rancoita@mib.infn.it

### ABSTRACT

A propagation model of galactic cosmic protons through the Heliosphere was implemented using a 2-D Monte Carlo approach to determine the differential intensities of protons during the solar cycle 23. The model includes the effects due to the variation of solar activity during the propagation of cosmic rays from the boundary of the heliopause down to Earth’s position. Drift effects are also accounted for. The simulated spectra were found in agreement with those obtained with experimental observations carried out by BESS, AMS and PAMELA collaborations. In addition, the modulated spectrum determined with the present code for the year 1995 exhibits the latitudinal gradient and equatorial southward offset minimum found by Ulysses fast scan in 1995.

*Subject headings:* Solar modulation, Interplanetary space, Cosmic rays propagation

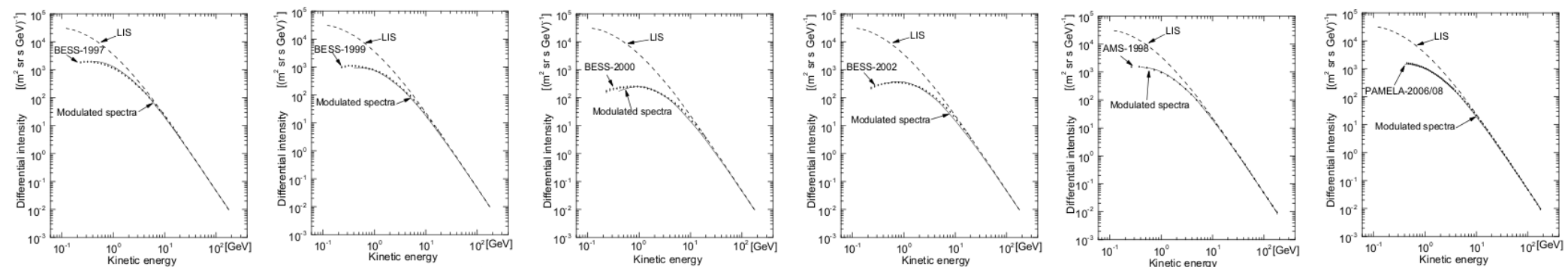
<sup>1</sup>Institute of Experimental Physics, Kosice (Slovak Republic).

<sup>2</sup>INFN, Milano-Bicocca, Milano (Italy).

<sup>3</sup>also Physics Department, University of Milano-Bicocca, Milano (Italy).

<sup>4</sup>also CILEA, Segrate (Milano, Italy).

<sup>5</sup>also University of Insubria, Como (Italy).



# HelMod – selected results

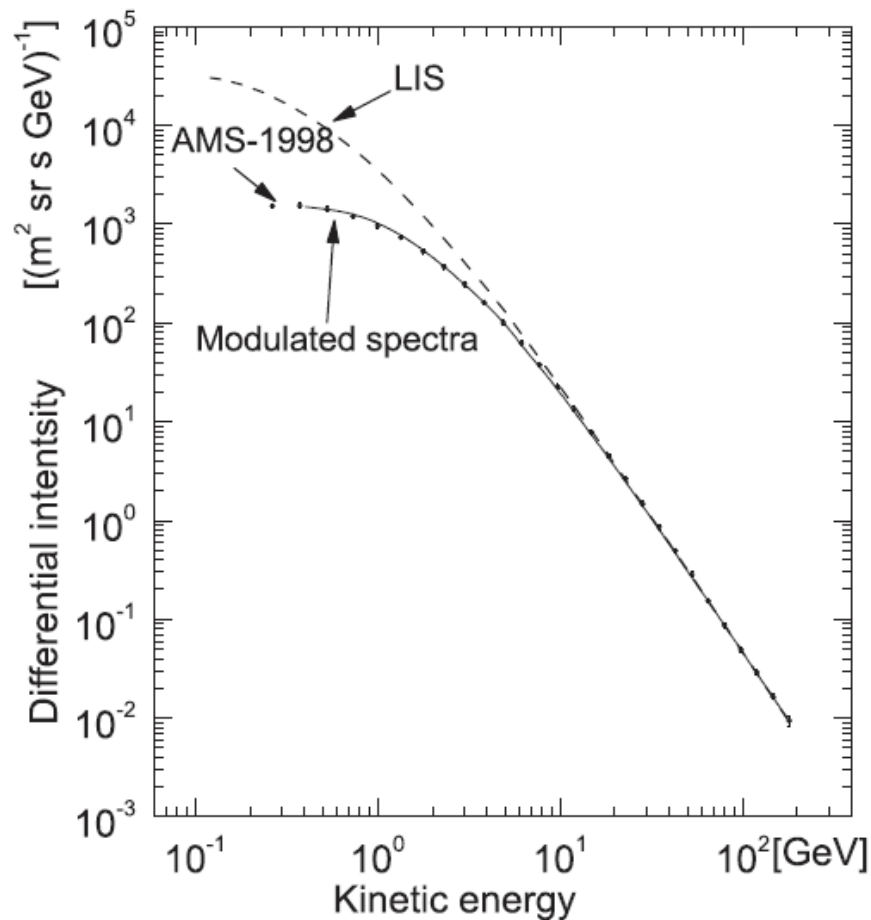


**Figure 8.** Differential intensity determined with the HelMod code (continuous line) compared to the experimental data of AMS–1998; the dashed line is the LIS (see the text).

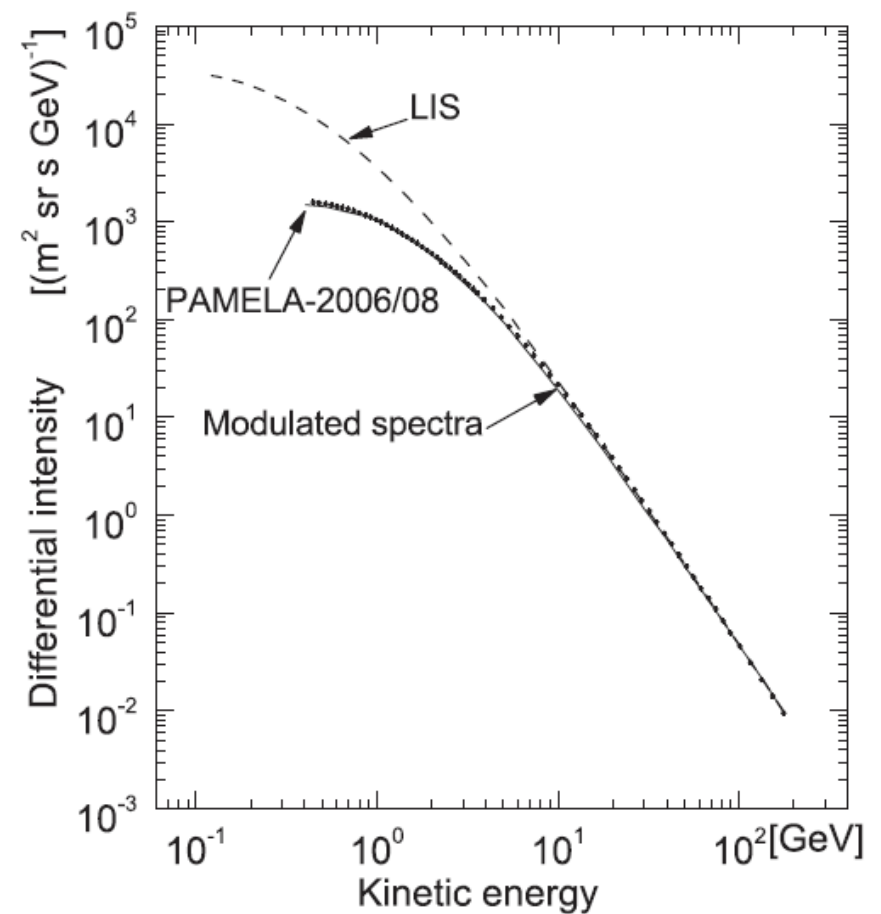
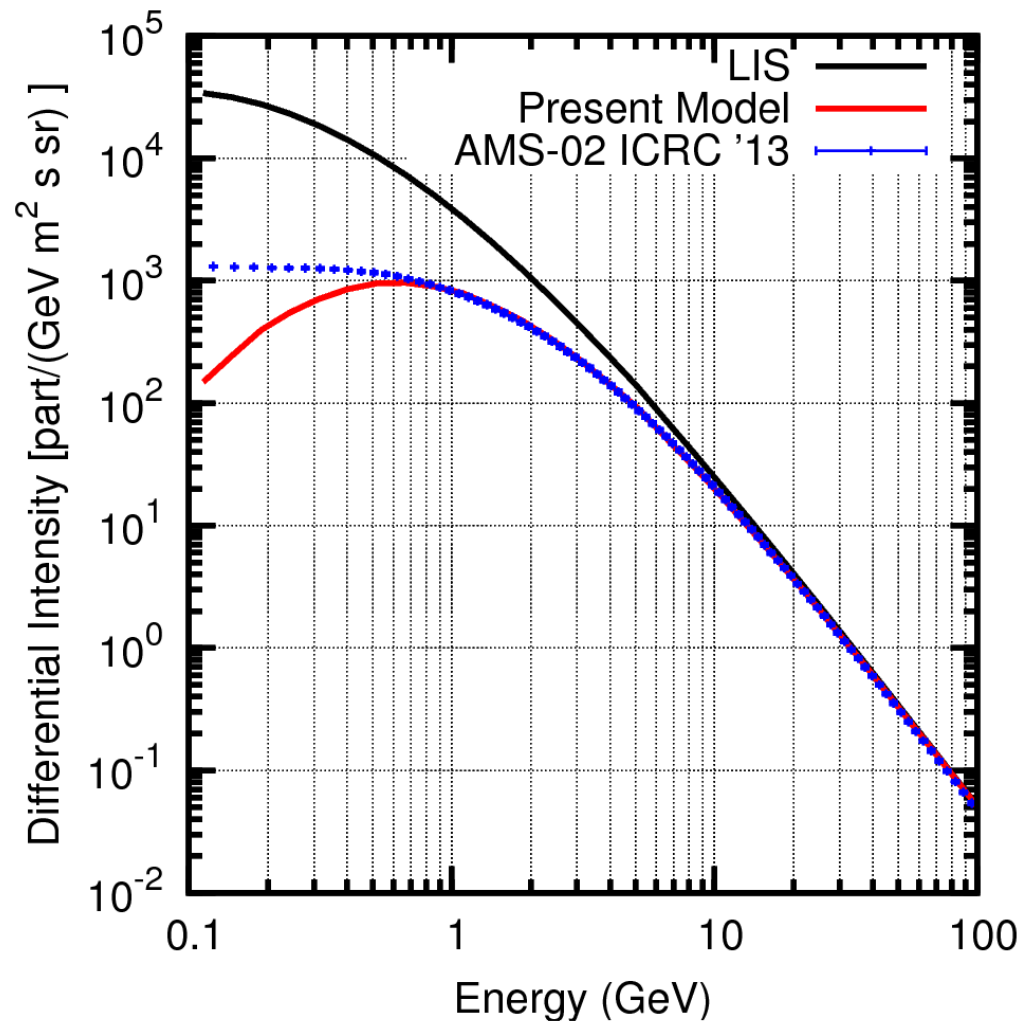


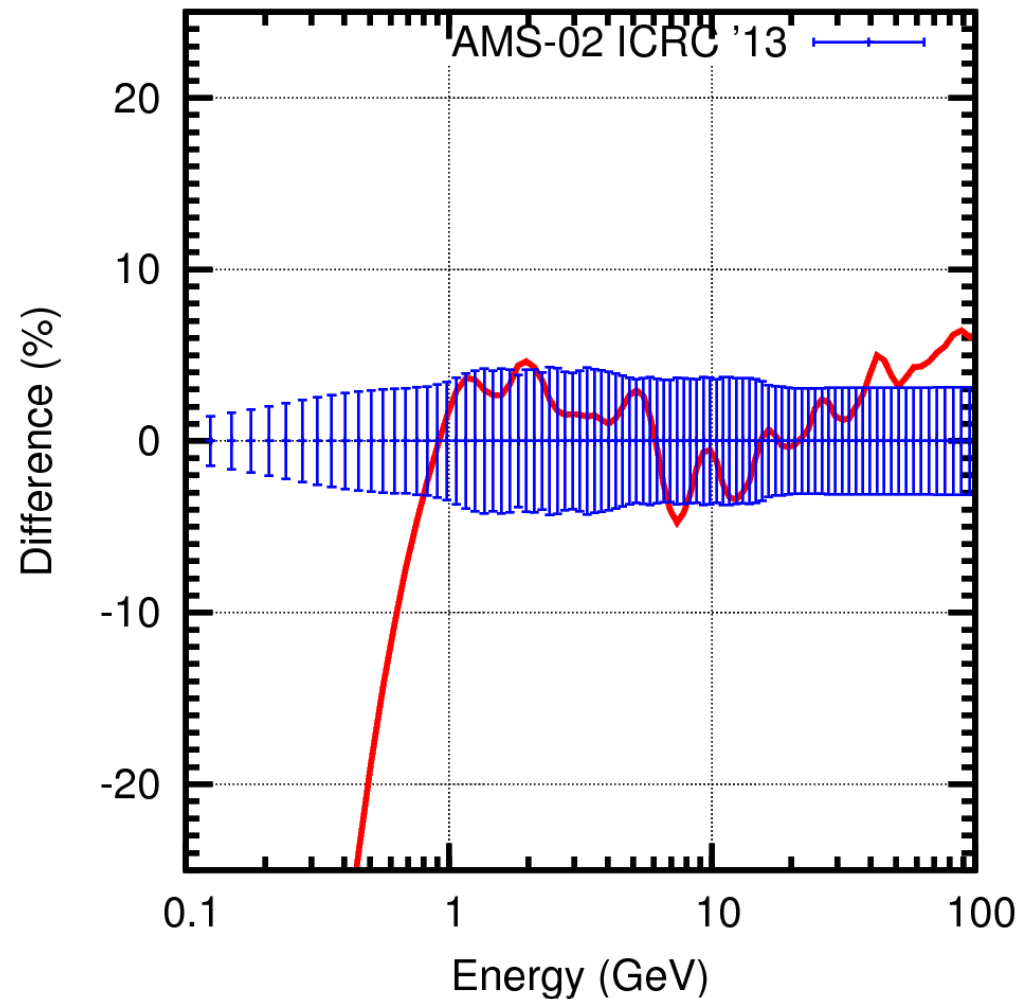
**Figure 10.** Differential intensity determined with the HelMod code (continuous line) compared to the experimental data of PAMELA–2006/08; the dashed line is the LIS (see the text).

# Results

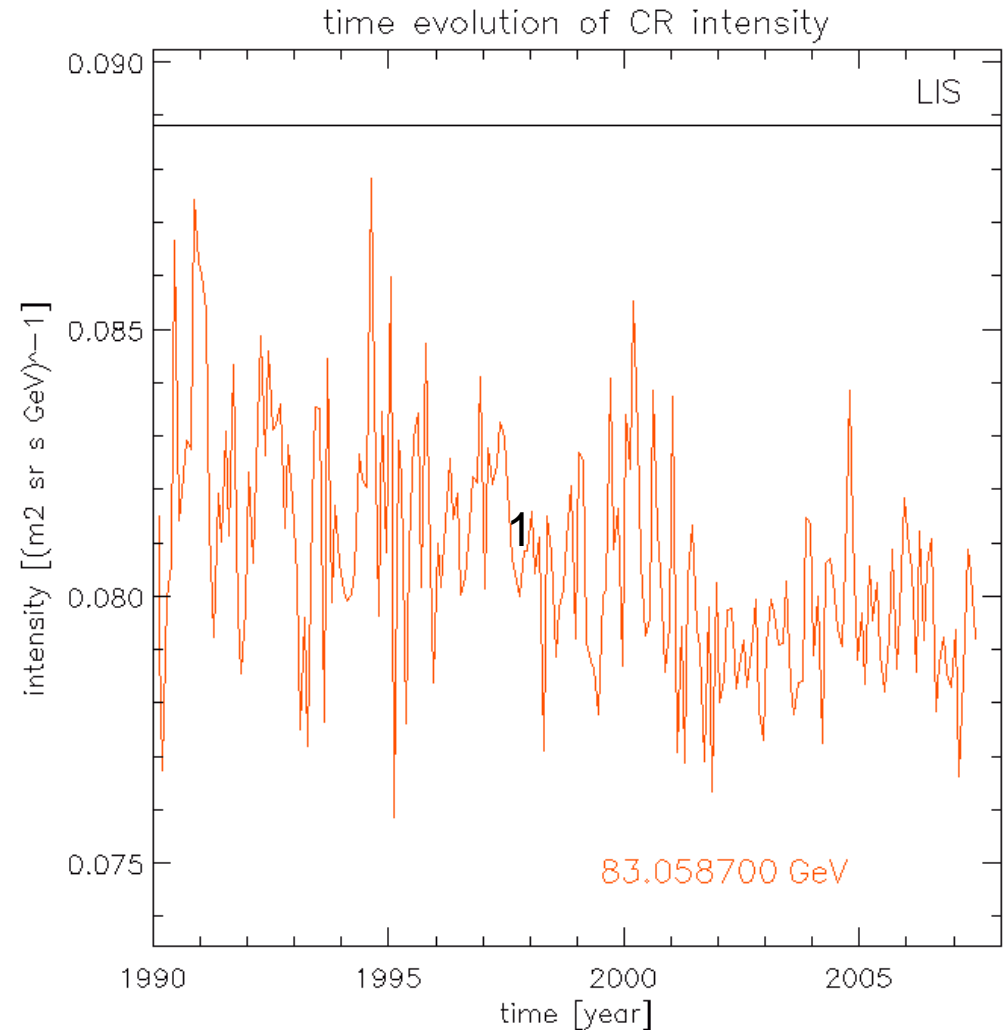
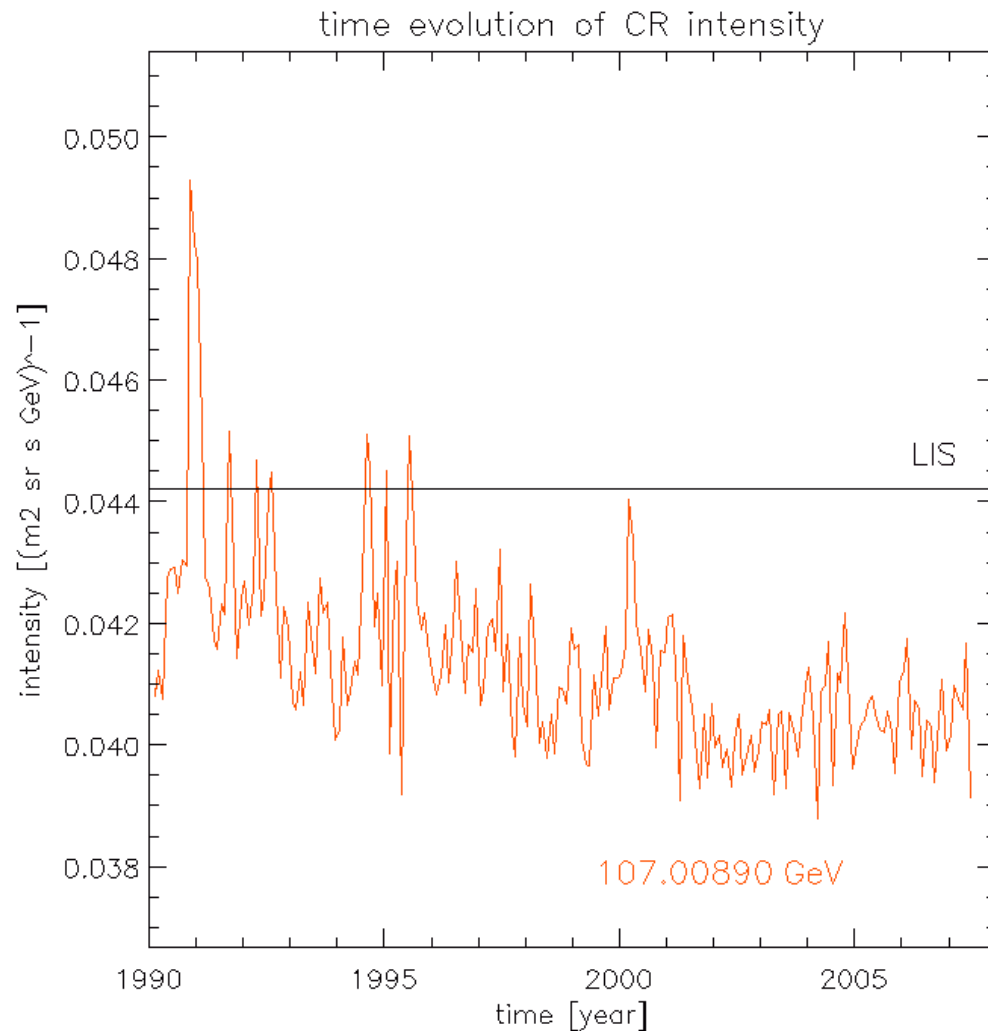
## AMS 02 vs. HelMod (2013)



- over 2 years average



# Some prediction of HelMod model



# HelMod – open questions

- over ~500 MeV (- 800 MeV) good agreement with experiments
- Why not on low energies?
  - Possible influence
    - ? modulation in heliosheat
    - ? shape of heliosphere (tail, north-south asymmetry)
    - ?? small anisotropy of GCR entering heliosphere ?
    - ? TS acceleration
    - ? LIS shape
    - ...

# Models selected results

## Comparison forward in time and backward in time methods to solve the cosmic rays transport equation in the heliosphere.

$$\frac{\partial U}{\partial t} = -\nabla \cdot (U\vec{V}) + \nabla \cdot [\vec{K} \cdot \nabla U] + \frac{(\nabla \cdot \vec{V})}{3} \frac{\partial}{\partial T} (\alpha_{\text{rel}} TU)$$

$$\frac{\partial f}{\partial t} = -\nabla \cdot (f\vec{V}) + \nabla \cdot [\vec{K} \cdot \nabla f] + \frac{(\nabla \cdot \vec{V})}{3p^2} \frac{\partial}{\partial p} (p^3 f)$$

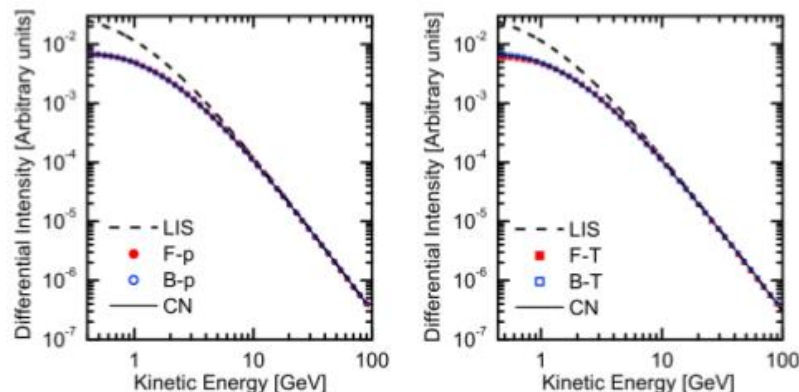


**Figure 2.** Particle differential intensity, in arbitrary units, at 1 AU evaluated by Monte Carlo and Crank-Nicolson methods. The LIS is shown as dashed line. CN is reported with black solid line. (left) **B-p** (blue round) and **F-p** (red round) solutions. (right) **B-T** (blue square) and **F-T** (red square) solutions.

### TECHNICAL REPORTS: METHODS

10.1002/2015JA022237

#### Key Points:

- Quantitative comparison of backward-forward-in-time cosmic rays transport Monte Carlo methods
- Estimation of systematic error of both methods for spectra at 1 AU for energies above 1 GV
- Backward-in-time method is suited for predicting modulated spectra for high-precision experiments

#### Correspondence to:

S. Della Torre and P. Bobik, stefano.dellatorre@mib.infn.it; bobik@saske.sk

#### Citation:

Bobik, P., et al. (2016), On the forward-backward-in-time approach for Monte Carlo solution of Parker's transport equation: One-dimensional case, *J. Geophys. Res. Space Physics*, 121, doi:10.1002/2015JA022237.

## On the forward-backward-in-time approach for Monte Carlo solution of Parker's transport equation: One-dimensional case

P. Bobik<sup>1</sup>, M. J. Boschini<sup>2,3</sup>, S. Della Torre<sup>2</sup>, M. Gervasi<sup>2,4</sup>, D. Grandi<sup>2</sup>, G. La Vacca<sup>2</sup>, S. Pensotti<sup>2,4</sup>, M. Putis<sup>1</sup>, P. G. Rancoita<sup>2</sup>, D. Rozza<sup>2,4</sup>, M. Tacconi<sup>2</sup>, and M. Zannoni<sup>2,4</sup>

<sup>1</sup>Institute of Experimental Physics, Slovak Academy of Sciences, Kosice, Slovakia, <sup>2</sup>INFN Sezione di Milano-Bicocca, Milan, Italy, <sup>3</sup>Cineca, Segrate, Italy, <sup>4</sup>Department of Physics, University of Milano-Bicocca, Milan, Italy

**Abstract** The cosmic rays propagation inside the heliosphere is well described by a transport equation introduced by Parker in 1965. To solve this equation, several approaches were followed in the past. Recently, a Monte Carlo approach became widely used in force of its advantages with respect to other numerical methods. In this approach the transport equation is associated to a fully equivalent set of stochastic differential equations (SDE). This set is used to describe the stochastic path of quasi-particle from a source, e.g., the interstellar space, to a specific target, e.g., a detector at Earth. We present a comparison of forward-in-time and backward-in-time methods to solve the cosmic rays transport equation in the heliosphere. The Parker equation and the related set of SDE in the several formulations are treated in this paper. For the sake of clarity, this work is focused on the one-dimensional solutions. Results were compared with an alternative numerical solution, namely, Crank-Nicolson method, specifically developed for the case under study. The methods presented are fully consistent each others for energy greater than 400 MeV. The comparison between stochastic integrations and Crank-Nicolson allows us to estimate the systematic uncertainties of Monte Carlo methods. The forward-in-time stochastic integrations method showed a systematic uncertainty <5%, while backward-in-time stochastic integrations method showed a systematic uncertainty <1% in the studied energy range.

IF= 3,318 Q1P

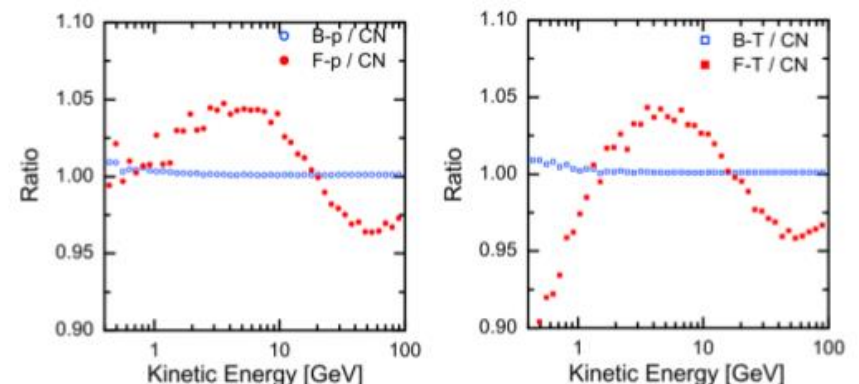


**Figure 3.** Ratio between Monte Carlo and CN solutions. (left) **B-p** over CN (blue round) and **F-p** over CN (red round) solutions. (right) **B-T** over CN (blue square) and **F-T** over CN (red square).



# New model of cosmic rays modulation in heliosphere

Monthly Notices

of the

ROYAL ASTRONOMICAL SOCIETY

MNRAS **470**, 1073–1085 (2017)

Advance Access publication 2017 May 16

doi:10.1093/mnras/stx1202

## An analytically iterative method for solving problems of cosmic-ray modulation

Yuriy L. Kolesnyk,<sup>1</sup>★ Pavol Bobik,<sup>2</sup>★ Boris A. Shakhov<sup>1</sup> and Marian Putis<sup>2</sup>

<sup>1</sup>Main Astronomical Observatory, National Academy of Sciences of Ukraine, 27, Akademika Zabolotnoho St., UA-03680 Kyiv, Ukraine

<sup>2</sup>Institute of Experimental Physics, Watsonova 47, 04001 Kosice, Slovakia

Accepted 2017 May 11. Received 2017 May 11; in original form 2017 February 13

### ABSTRACT

The development of an analytically iterative method for solving steady-state as well as unsteady-state problems of cosmic-ray (CR) modulation is proposed. Iterations for obtaining the solutions are constructed for the spherically symmetric form of the CR propagation equation. The main solution of the considered problem consists of the zero-order solution that is obtained during the initial iteration and amendments that may be obtained by subsequent iterations. The finding of the zero-order solution is based on the CR isotropy during propagation in the space, whereas the anisotropy is taken into account when finding the next amendments. To begin with, the method is applied to solve the problem of CR modulation where the diffusion coefficient  $\kappa$  and the solar wind speed  $u$  are constants with an Local Interstellar Spectra (LIS) spectrum. The solution obtained with two iterations was compared with an analytical solution and with numerical solutions. Finally, solutions that have only one iteration for two problems of CR modulation with  $u = \text{constant}$  and the same form of LIS spectrum were obtained and tested against numerical solutions. For the first problem,  $\kappa$  is proportional to the momentum of the particle  $p$ , so it has the form  $\kappa = k_0 \eta$ , where  $\eta = \frac{p}{m_0 c}$ . For the second problem, the diffusion coefficient is given in the form  $\kappa = k_0 \beta \eta$ , where  $\beta = \frac{v}{c}$  is the particle speed relative to the speed of light. There was a good matching of the obtained solutions with the numerical solutions as well as with the analytical solution for the problem where  $\kappa = \text{constant}$ .

**Key words:** methods: analytical – Sun: heliosphere – cosmic rays.

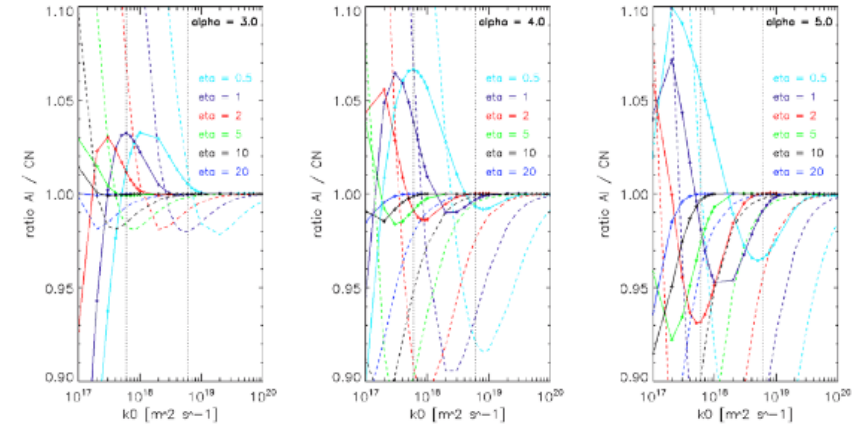


**Figure 8.** The comparison of the ratio of the AI and CN solutions for different diffusion coefficients  $k_0$  and  $\alpha = 3$  (left-hand panel), 4 (middle panel) and 5 (right-hand panel) at 1 au for  $\eta = 0.5, 1, 2, 5, 10, 20$ . Dashed lines represent the ratio  $AI(N_0)/CN$  and solid lines represent the ratio  $AI(N_0 + N_1)/CN$ . AI and CN for  $\kappa = k_0 \beta \eta$  (for more details, see the text)

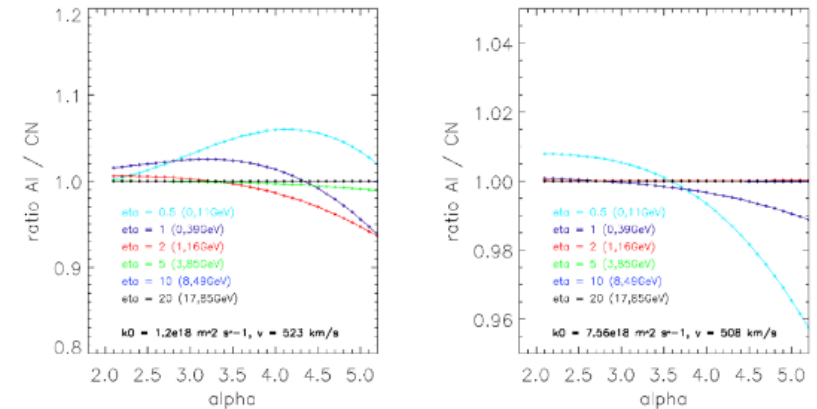


**Figure 9.** The comparison of the ratio of the AI and CN solutions as functions of the initial spectrum slope  $\alpha$  at 1 au for two selected values of  $k_0$ . Solutions for  $\kappa = k_0 \beta \eta$  (for more details, see the text).

# APPENDIX C: $\kappa = k_0 \beta \eta$

To obtain a solution for the problem, we introduce the following dimensionless variables:  $x = \frac{ur}{k_0}$ ,  $x_0 = \frac{ur_0}{k_0}$  and  $\eta = \frac{p}{m_0 c}$ . Note that for such a problem, the diffusion coefficient  $\kappa$  can be rewritten in the following form:  $\kappa = k_0 \frac{\eta^2}{\sqrt{\eta^2+1}}$ . This follows from the fact that  $p = \frac{VE}{c^2}$  and  $E = \sqrt{p^2 c^2 + m_0^2 c^4}$ . Taking into account (6) and (9), we obtain a system of equations for finding the zero-order solution:

$$\begin{cases} \frac{\eta}{\sqrt{\eta^2+1}} \frac{\partial N_0(x, \eta)}{\partial x} + \frac{1}{3} \frac{\partial N_0(x, \eta)}{\partial \eta} = 0, \\ N_0(x_0, \eta) = A \eta^{-\alpha}. \end{cases} \quad (C1)$$

The last system can be rewritten in the form

$$\begin{cases} N_0(x, \eta) = f(\sqrt{\eta^2+1} - \frac{x}{3}), \\ N_0(x_0, \eta) = A \eta^{-\alpha}. \end{cases} \quad (C2)$$

Then, the solution of the last system has the form

$$N_0 = A \left( \sqrt{\left[ \sqrt{\eta^2+1} - \frac{x-x_0}{3} \right]^2 - 1} \right)^{-\alpha}. \quad (C3)$$

After inserting  $N_0$  into (11), we will obtain an equation for  $N_1$ :

$$\begin{aligned} \frac{1}{x^2} \frac{\partial}{\partial x} x^2 \left[ \frac{\eta^2}{\sqrt{\eta^2+1}} \frac{\partial N_1}{\partial x} + \frac{\eta}{3} \frac{\partial N_1}{\partial \eta} \right] \\ = -\frac{\alpha A}{3} \left( \left[ \sqrt{\eta^2+1} - \frac{x-x_0}{3} \right]^2 - 1 \right)^{-\frac{\alpha}{2}-1} \left[ \sqrt{\eta^2+1} - \frac{x-x_0}{3} + \frac{\eta^2}{3\sqrt{\eta^2+1}} \frac{(\alpha+1)(\sqrt{\eta^2+1} - \frac{x-x_0}{3})^2 + 1}{1 - (\sqrt{\eta^2+1} - \frac{x-x_0}{3})^2} \right]. \end{aligned} \quad (C4)$$

After introducing the variable:  $\theta = \sqrt{\eta^2+1}$  and simplifying the last equation, we obtain

$$-\frac{\partial N_1}{\partial x} - \frac{1}{3} \frac{\partial N_1}{\partial \theta} = -\frac{\alpha A}{3x^2(\theta^2-1)} \left[ \left( \frac{4\theta^2-1}{3} + \frac{x_0\theta}{3} \right) K - \frac{\theta}{3} L - \frac{(\alpha+2)(\theta^2-1)}{3} M \right], \quad (C5)$$

where

$$\begin{aligned} K &= \int_0^x \left( \left[ \theta - \frac{x-x_0}{3} \right]^2 - 1 \right)^{-\frac{\alpha}{2}-1} x^2 dx; \\ L &= \int_0^x \left( \left[ \theta - \frac{x-x_0}{3} \right]^2 - 1 \right)^{-\frac{\alpha}{2}-1} x^3 dx; \\ M &= \int_0^x \left( \left[ \theta - \frac{x-x_0}{3} \right]^2 - 1 \right)^{-\frac{\alpha}{2}-2} \left[ \theta - \frac{x-x_0}{3} \right]^2 x^2 dx. \end{aligned}$$

Note that the limits of integration in  $K$ ,  $L$ ,  $M$  were selected as being from 0 to  $x$  in consequence of applying the first condition (12). The detailed calculation of the integrals was explained in Appendix D.

Due to the fact that the solution of the homogeneous equation (C5) has the form  $f(\theta - \frac{x}{3})$ , and taking into account the second condition (12), it is necessary to search for an  $N_1$  in the following form:

$$N_1 = \int_x^{x_0} f \left( x \rightarrow \xi, \theta \rightarrow \theta - \frac{x-\xi}{3} \right) d\xi. \quad (C6)$$

By taking into account the form for  $N_1$  (C6) and also using (C5), we obtain

$$\begin{aligned} N_1 &= -\frac{\alpha A}{9} \int_x^{x_0} \frac{d\xi}{\xi^2 \left( \left( \theta - \frac{x-\xi}{3} \right)^2 - 1 \right)} \left[ \left( 4 \left( \theta - \frac{x-\xi}{3} \right)^2 + x_0 \left( \theta - \frac{x-\xi}{3} \right) - 1 \right) K \left( x \rightarrow \xi, \theta \rightarrow \theta - \frac{x-\xi}{3} \right) - \left( \theta - \frac{x-\xi}{3} \right) \right. \\ &\quad \times L \left( x \rightarrow \xi, \theta \rightarrow \theta - \frac{x-\xi}{3} \right) - (\alpha+2) \left( \left( \theta - \frac{x-\xi}{3} \right)^2 - 1 \right) M \left( x \rightarrow \xi, \theta \rightarrow \theta - \frac{x-\xi}{3} \right) \left. \right]. \end{aligned} \quad (C7)$$

$$K = k_0 \beta \eta$$

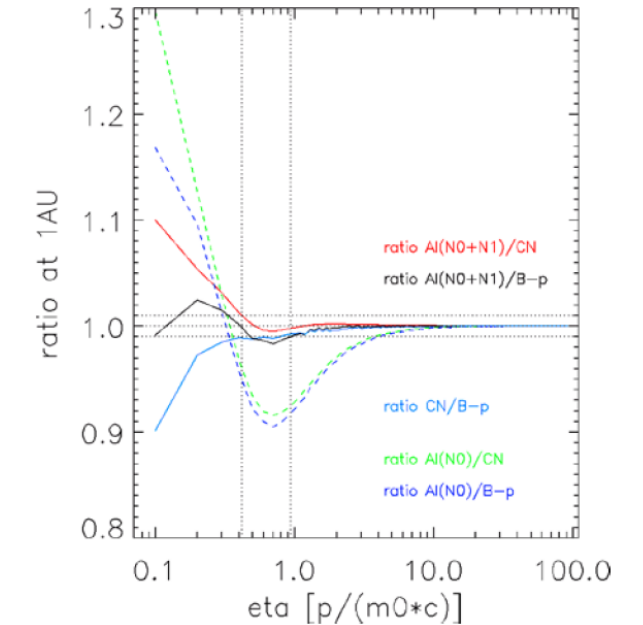
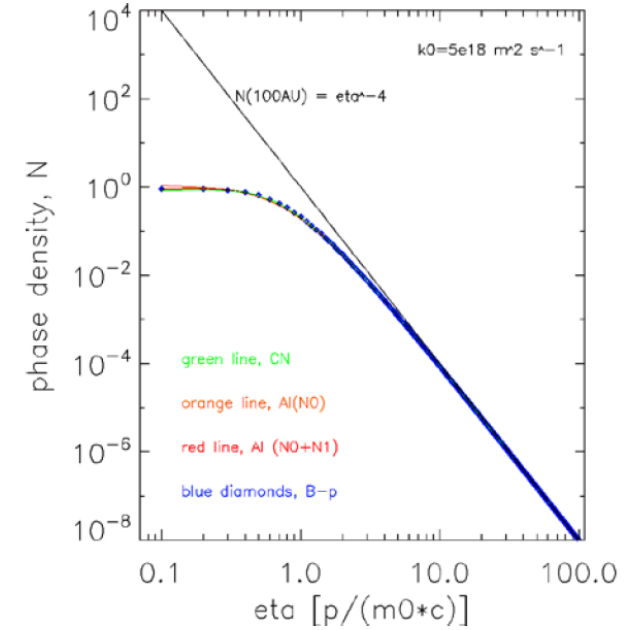


**Figure 7.** The comparison of the Al, B-p and CN solutions at 1 au for  $k_0 = 5 \times 10^{18} \text{ m}^{-2} \text{ s}^{-1}$ ,  $\alpha = 4.0$  and  $\kappa = k_0 \beta \eta$  (for more details, see the text)



## APPENDIX D: CALCULATION OF THE INTEGRALS $K$ , $L$ , $M$

For the calculation of the integrals  $K$ ,  $L$ ,  $M$  from Appendix C, let us first consider the integral  $I$  that has the following form:

$$I = \int z^k (z^2 - 1)^\beta dz. \quad (D1)$$

If we represent  $(z^2 - 1)^\beta$  as a sum, i.e.  $(z^2 - 1)^\beta = \sum_{n=0}^{\infty} (-1)^n C_\beta^n \cdot (z^2)^{\beta-n}$ , where  $C_\beta^n$  is the binomial coefficient (which can be represented through the Gamma function  $\Gamma$  as  $C_\beta^n = \frac{\Gamma(\beta+1)}{\Gamma(\beta-n+1)n!}$ ), we can apply here properties of  $\Gamma$  such as  $\frac{\Gamma(\beta+1)}{\Gamma(\beta-n+1)} = \frac{\Gamma(n-\beta)}{\Gamma(-\beta)} (-1)^n$  and see that  $I$  assumes the following form:

$$I = -\frac{z^{k+2\beta+1}}{2} \sum_{n=0}^{\infty} \frac{\Gamma(n-\beta)}{\Gamma(-\beta)n!(n-\beta-\frac{k}{2}-\frac{1}{2})} z^{-2n}. \quad (D2)$$

If we now use the fact that  $\Gamma(z) = z\Gamma(z+1)$  and multiply (D2) by  $\frac{\Gamma(-\frac{k}{2}+\frac{1}{2}-\beta)}{\Gamma(-\frac{k}{2}-\frac{1}{2}-\beta)}$ , then we obtain

$$I = -\frac{z^{k+2\beta+1}}{2} \frac{\Gamma(-\frac{k}{2}-\frac{1}{2}-\beta)}{\Gamma(-\frac{k}{2}+\frac{1}{2}-\beta)} \sum_{n=0}^{\infty} \frac{\Gamma(-\beta+n)\Gamma(n-\frac{k}{2}-\frac{1}{2}-\beta)\Gamma(-\frac{k}{2}+\frac{1}{2}-\beta)}{\Gamma(-\beta)n!\Gamma(n-\frac{k}{2}+\frac{1}{2}-\beta)\Gamma(-\frac{k}{2}-\frac{1}{2}-\beta)} z^{-2n}. \quad (D3)$$

For the last expression, we can apply the definition of hypergeometrical function  $F(a, b; c; z)$  (Bateman & Erdelyi 1953):  $F(a, b; c; z) = \sum_{n=0}^{\infty} \frac{\Gamma(a+n)}{\Gamma(a)} \frac{\Gamma(b+n)}{\Gamma(b)} \frac{\Gamma(c)}{\Gamma(c+n)} \frac{z^n}{n!}$ . Finally, we obtain

$$\int z^k (z^2 - 1)^\beta dz = \frac{z^{k+1+2\beta}}{k+1+2\beta} F(-\beta, -\frac{k}{2}-\frac{1}{2}-\beta; -\frac{k}{2}+\frac{1}{2}-\beta; z^{-2}). \quad (D4)$$

And now, to use (D4) to find the integrals  $K$ ,  $L$ ,  $M$ , we substitute  $\theta - \frac{x-x_0}{3} = z$  in these integrals. As a result, these integrals take the following form:

$$\begin{aligned} K &= 27 \int_{\theta - \frac{x-x_0}{3}}^{\theta + \frac{x_0}{3}} (z^2 - 1)^{-\frac{\alpha}{2}-1} (z^2 - 2\omega z + \omega^2) dz; \\ L &= -81 \int_{\theta - \frac{x-x_0}{3}}^{\theta + \frac{x_0}{3}} (z^2 - 1)^{-\frac{\alpha}{2}-1} (z^3 - 3\omega z^2 + 3\omega^2 z - \omega^3) dz; \\ M &= 27 \int_{\theta - \frac{x-x_0}{3}}^{\theta + \frac{x_0}{3}} (z^2 - 1)^{-\frac{\alpha}{2}-2} (z^4 - 2\omega z^3 + \omega^2 z^2) dz, \end{aligned}$$

where  $\omega = \theta + \frac{x_0}{3}$ . Eventually, if we apply (D4) to each of these integrals, we obtain

$$\begin{aligned} K &= \left[ \frac{27}{1-\alpha} z^{1-\alpha} F\left(\frac{\alpha}{2}+1, \frac{\alpha}{2}-\frac{1}{2}; \frac{\alpha}{2}+\frac{1}{2}; \frac{1}{z^2}\right) + \frac{54}{\alpha} \omega z^{-\alpha} F\left(\frac{\alpha}{2}+1, \frac{\alpha}{2}; \frac{\alpha}{2}+1; \frac{1}{z^2}\right) \right. \\ &\quad \left. - \frac{27}{\alpha+1} \omega^2 z^{-\alpha-1} F\left(\frac{\alpha}{2}+1, \frac{\alpha}{2}+\frac{1}{2}; \frac{\alpha}{2}+\frac{3}{2}; \frac{1}{z^2}\right) \right]_{\theta - \frac{x-x_0}{3}}^{\theta + \frac{x_0}{3}}, \end{aligned} \quad (D5)$$

$$\begin{aligned} L &= \left[ \frac{81}{\alpha-2} z^{2-\alpha} F\left(\frac{\alpha}{2}+1, \frac{\alpha}{2}-1; \frac{\alpha}{2}; \frac{1}{z^2}\right) + \frac{243}{1-\alpha} \omega z^{1-\alpha} F\left(\frac{\alpha}{2}+1, \frac{\alpha}{2}-\frac{1}{2}; \frac{\alpha}{2}+\frac{1}{2}; \frac{1}{z^2}\right) \right. \\ &\quad \left. + \frac{243}{\alpha} \omega^2 z^{-\alpha} F\left(\frac{\alpha}{2}+1, \frac{\alpha}{2}; \frac{\alpha}{2}+1; \frac{1}{z^2}\right) - \frac{81}{\alpha+1} \omega^3 z^{-\alpha-1} F\left(\frac{\alpha}{2}+1, \frac{\alpha}{2}+\frac{1}{2}; \frac{\alpha}{2}+\frac{3}{2}; \frac{1}{z^2}\right) \right]_{\theta - \frac{x-x_0}{3}}^{\theta + \frac{x_0}{3}}, \end{aligned} \quad (D6)$$

$$\begin{aligned} M &= \left[ \frac{27}{-\alpha+1} z^{-\alpha+1} F\left(\frac{\alpha}{2}+2, \frac{\alpha}{2}-\frac{1}{2}; \frac{\alpha}{2}+\frac{1}{2}; \frac{1}{z^2}\right) + \frac{54}{\alpha} \omega z^{-\alpha} F\left(\frac{\alpha}{2}+2, \frac{\alpha}{2}; \frac{\alpha}{2}+1; \frac{1}{z^2}\right) \right. \\ &\quad \left. - \frac{27}{\alpha+1} \omega^2 z^{-\alpha-1} F\left(\frac{\alpha}{2}+2, \frac{\alpha}{2}+\frac{1}{2}; \frac{\alpha}{2}+\frac{3}{2}; \frac{1}{z^2}\right) \right]_{\theta - \frac{x-x_0}{3}}^{\theta + \frac{x_0}{3}}. \end{aligned} \quad (D7)$$

$$K = k_0 \beta \eta$$

# IEP SAS Department of Space Physics: Detached Laboratory at Lomnický štít (LS)

Long term measurement of cosmic rays (CR) by neutron monitor (NM) with high statistics and temporal resolution at LS (2636 m. a.s.l. 1982-2015) allowed in last years to :

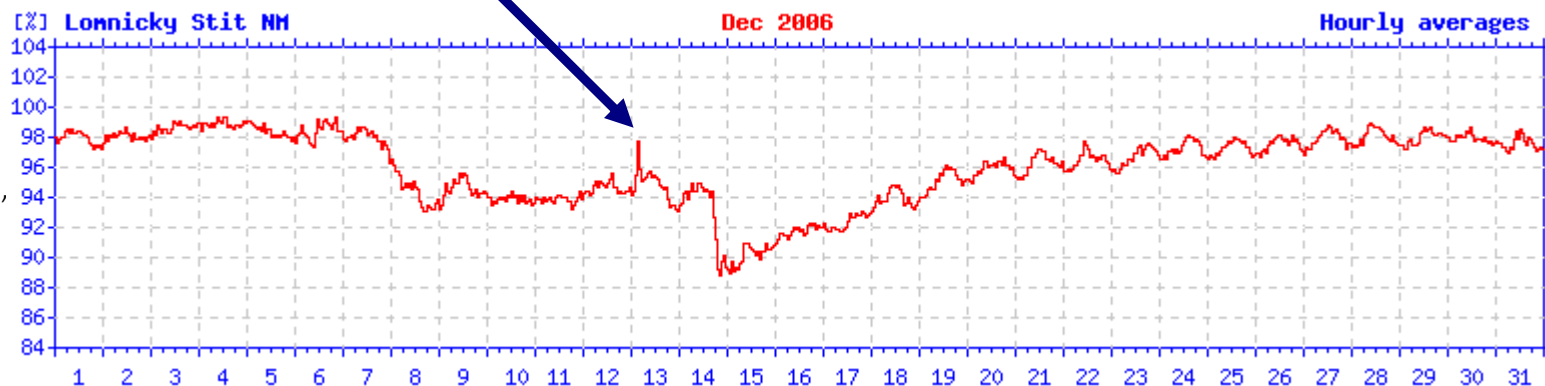
- describe the quasi-periodic variations of CR intensity in wide frequency range [2];
- obtain relations between CR decreases (FDs), parameters of interplanetary medium and geomagnetic activity at middle latitudes [1] ; to find that cloudiness at LS may have marginal relation to CR intensity [3]
- find that particles accelerated during GLE 70 caused the changes in VLF electromagnetic wave transmission between Europe and America on the night side of Earth [5]
- estimate possibilities of dosimetric measurements at LS during changes of primary CR intensity [4]. Data continuously utilized as one of the features of space weather state monitoring (e.g. for estimate of radiation dose at airplane altitudes).

## References

1. Parnahaj I., Kudela K., Astrophys. Space Sci., 359, 1, 35-35, 2015
2. Kudela K., Langer R., Rad. Protect. Dosim., 164, 4, 471-476, 2015
3. Kancířová M., Kudela K., Atmos. Res., 149, 166-173, 2014
4. Kubančák J. et al. J. Instrumentation, 9, 7018-7018, 2014
5. Zigman V., Kudela K., Grubor D. Adv. Space Res., 53, 5, 763-775, 2014



LS (2634 m above sea) - suitable location for CR observations. Measurements by NM, in real time <http://neutronmonitor.ta3.sk>, in network: <http://nmdb.eu>, and by SEVAN, in network: [http://crd.yerphi.am/Lomnicky\\_stit\\_SEVAN\\_Data](http://crd.yerphi.am/Lomnicky_stit_SEVAN_Data)



# Secondary cosmic rays and electric fields at Lomnický štít

 **AGU** PUBLICATIONS



**Journal of Geophysical Research: Atmospheres**

## RESEARCH ARTICLE

10.1002/2016JD026439

### Key Points:

- Short-term (minutes to tens of minutes) increases in the upper scintillator of SEVAN detector system at altitude 2,634 m are observed
- Increases correspond to periods of high electric field measured at the same site rather than with the individual discharges (lightning)
- Increases during thunderstorm period in 2016 correspond with higher probability to negative rather than to positive vertical electric field

### Supporting Information:

- Supporting Information S1

### Correspondence to:

K. Kudela,  
kkudela@saske.sk

## Correlations Between Secondary Cosmic Ray Rates and Strong Electric Fields at Lomnický štít

K. Kudela<sup>1,2</sup> , J. Chum<sup>3</sup> , M. Kollárik<sup>1</sup>, R. Langer<sup>1</sup>, I. Strhárský<sup>1</sup>, and J. Baše<sup>3</sup>

<sup>1</sup>Institute of Experimental Physics, Slovak Academy of Sciences, Košice, Slovakia, <sup>2</sup>Nuclear Physics Institute of the CAS, Řež, Czech Republic, <sup>3</sup>Institute of Atmospheric Physics of the CAS, Prague, Czech Republic

**Abstract** Since March 2014, there is a continuous measurement of secondary cosmic rays by the detector system SEVAN (Space Environmental Viewing and Analysis Network) at Lomnický štít, altitude 2,634 m above sea level. Starting from June 2016, the count rates (1 s resolution) obtained from the three SEVAN detectors and from their coincidences are available, along with selected meteorological characteristics. Since 30 May 2016 the electric field measurements have been installed at the same site. Several events with clear increase of the count rate in the upper detector of SEVAN were observed during the thunderstorms until 17 September 2016. Examples of these measurements are presented and discussed. Barometric pressure correction and elimination of low-frequency variability from the signal allow to extract 2 min averaged increases from the data. It is shown that the 2 min averaged increases of count rates measured by SEVAN correspond with periods of high electric field (with higher probability during negative polarity) rather than with the individual discharges (lightning).



## DOK-M



Device name: DOK-M

Project name: RESONANCE

Space probe: RESONANCE

Space launcher: Soyuz-2-1B/Fregat

Spaceport: Baikonur

Launch date: 2022?

Pericentre [km]: 500

Apocentre [km]: 27375

Inclination [°]: 63,41°

Orbital period: 8 h

Orientation: heliocentric

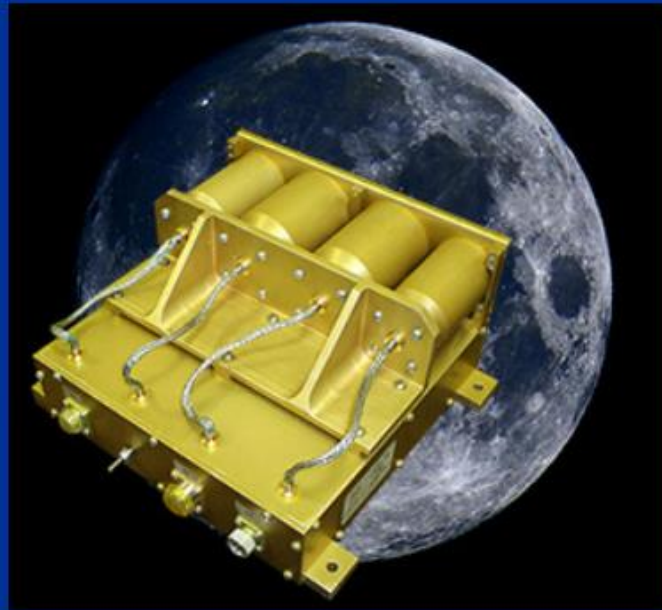
The project RESONANCE is a magnetospheric space exploration mission dedicated for advanced study of the wave – particle interactions in the Earth's magnetosphere. Earth's magnetosphere, as natural resonator for many types of electromagnetic waves, is a place where electromagnetic waves efficiently interact with charged energetic particles via cyclotron resonance. The project RESONANCE is conducted by **Space Research Institute (IKI-RAN)** in Moscow, Russian Federation.

The DOK-M is a scientific space device dedicated for charged energetic particles temporal and energy sampling on board of two cooperating spacecraft of the RESONANCE project, presently under development at laboratories of IEP-SAS. The DOK-M is a joint international scientific space project of IEP-SAS, **Democritus University of Thrace, Greece** and **Space Research Institute (IKI)** in Moscow.



The DOK-M spectrometer is equipped with four passive cooled silicon solid state detectors, two of them are dedicated for detection of the energetic ions, another two detect the energetic electrons. The device is powered from 27 V onboard power distribution and communicates with onboard telemetry system by 125 kbps serial link.

## ASPECT-L



Device name: ASPECT-L  
Project name: LUNA-GLOBE  
Space probe: LUNA-GLOBE  
Space launcher: Soyuz  
Spaceport: Baykonur  
Launch date: 2020  
Pericentre [km]: tbd  
Apocentre [km]: tbd  
Inclination [°]: tbd  
Orbital period: tbd  
Orientation:

The project LUNA-GLOBE is a space exploration mission dedicated for advanced study of Moon and its environment. The project LUNA-GLOBE is conducted by **Space Research Institute (IKI-RAN)** in Moscow, Russian Federation.

The ASPECT-L is a scientific space device dedicated for charged energetic particles temporal and energy sampling on board of lunar orbiter. ASPECT-L is presently under development at laboratory of space technology of DSP-IEP-SAS. The ASPECT-L is a joint international scientific space project of IEP-SAS, **Democritus University of Thrace, Greece** and **Space Research Institute (IKI)** in Moscow.



The ASPECT-L is equipped with four passive cooled silicon solid state detectors (SSD), two of them are dedicated for detection of the energetic ions, another two detect the energetic electrons. The device is powered from 27 V onboard power distribution and communicates with onboard telemetry system by 1 Mbps serial link.



## PICAM



Device name: SERENA / PICAM

Project name: BepiColombo

Space probe: BepiColombo

Space launcher: Ariane 5

Spaceport: Kourou

Launch date: Oct. 2018

Pericentre [km]: tbd

Apocentre [km]: tbd

Inclination [°]: tbd

Orbital period: tbd

Orientation:

The project BepiColombo is a planetary exploration mission dedicated for advanced study of the planet Mercury, conducted by European Space Agency **ESA** and Japanese Space Agency **JAXA**.

Development of PICAM is conducted by Space Research Institute **IWF** (Institut für Weltraumforschung) in Graz, Austria, in wide international collaboration with many renowned laboratories of space research.



PICAM will provide the mass composition, energy and angular distribution of low energy ions up to 3 keV in the environment of planet Mercury.

The Department of Space physics IEP-SAS contributes to PICAM construction in the frame of scientific-technical cooperation with STIL-NUIM, Maynooth, Ireland.



Some Slovak industrial companies are also contributing as subcontractors to PICAM construction. The **Q-Products** company is acknowledged by PICAM team for precision manufacture of mechanical parts on 5-axis CNC centre and by laser technology.

## PEP / JDC



Device name: PEP / JDC

Project name: ESA-JUICE

Space probe: ESA-JUICE

Space launcher: Ariane 5

Spaceport: Kourou

Launch date: 2022

Pericentre [km]: tbd

Apocentre [km]: tbd

Inclination [°]: tbd

Orbital period: tbd

Orientation:

Project **JUICE (JUPiter ICy moons Explorer)** is a mission of European space agency **ESA** to planet Jupiter and its moons Europa, Ganymede and Callisto. The probe will orbit Jupiter and at the end of the mission it will orbit the moon Ganymede.



The Department of Space Physics IEP-SAS contributes to development and construction of particle detection science suite PEP (Particle Environment Package) and particularly its plasma analyzer JDC (Jovian plasma Dynamics and Composition) in the frame of scientific-technical collaboration with Swedish Institute of Space Physics **IRF** in Kiruna.



# JEM-EUSO

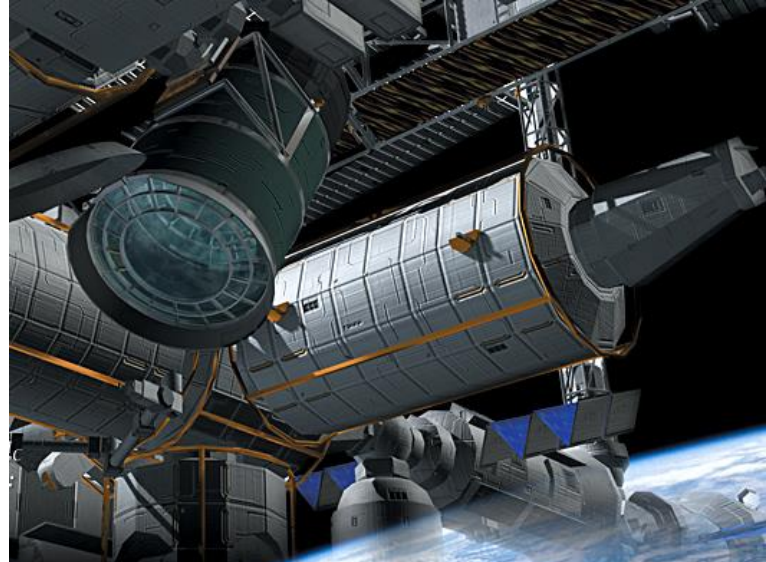
Extreme Universe Space Observatory onboard Japanese Experiment Module on ISS

Slovakia member since 2008 (IEP SAS, TUKE since 2015)

16 countries

93 institutes

more than 300 researchers

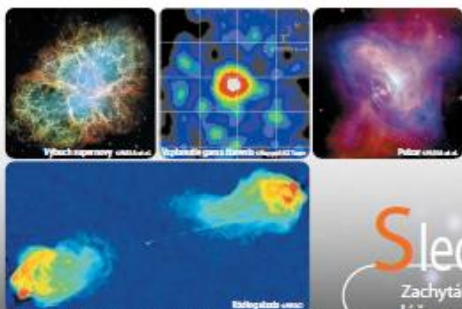


## Genéza

Najvyššie energie nad  $10^{20}$  eV pozorované vo svete

Takže nabitých častíc rastie na Zemi, každú sekundu na každý  $m^2$ . So zvyšujúcou sa energiou častíc, ich traja klesá so zvyšovaním energie častíc. Odkiaľ sa, že prichádzajúca nabitá častica s energiou nad  $4 \times 10^{19}$  eV budú existovať? Generálna strata pri spozorovaní kozmických častíc s energiou nad  $10^{20}$  eV. Po objavení častíc s energiou  $10^{20}$  eV v roku 1962. Uskutočnením, ktoré nových častíc, a podrobným sledovaním boli spozorované v 90. rokoch v projektoch Akeno-Giant Air Shower Array (AGASA) na Univerzite v Tokyu a Tj/ Ene16-Res Experiment-om na Univerzite v Utahu. Pôvod vysokoenergetických častíc je neznámy a fascinujúci, a pokiaľ možno vedecky záujem.

1) "MPL" - 16. Medzinárodná vesmírna stanica (ISS) - 16. Medzinárodná vesmírna stanica (ISS)



1) Každá 10. sekunda nabitá častica s energiou nad  $10^{20}$  eV padá na Zem.

## Sledovanie

Zachytávanie ultrafialových lúčov z atmosférickej spršky

Nabitá častica dopadajúca na zemskú atmosféru sa rozkladá a vytvára atmosférickú spršku. Táto sprška sa rozkladá na častice, ktoré sú viditeľné ako svetlo. Častice s energiou nad  $10^{20}$  eV vytvárajú atmosférickú spršku, ktorá sa rozkladá na častice, ktoré sú viditeľné ako svetlo. Častice s energiou nad  $10^{20}$  eV vytvárajú atmosférickú spršku, ktorá sa rozkladá na častice, ktoré sú viditeľné ako svetlo.

Častice v atmosférickej sprške sú viditeľné ako svetlo. Častice s energiou nad  $10^{20}$  eV vytvárajú atmosférickú spršku, ktorá sa rozkladá na častice, ktoré sú viditeľné ako svetlo. Častice s energiou nad  $10^{20}$  eV vytvárajú atmosférickú spršku, ktorá sa rozkladá na častice, ktoré sú viditeľné ako svetlo.

Častice s energiou nad  $10^{20}$  eV vytvárajú atmosférickú spršku, ktorá sa rozkladá na častice, ktoré sú viditeľné ako svetlo. Častice s energiou nad  $10^{20}$  eV vytvárajú atmosférickú spršku, ktorá sa rozkladá na častice, ktoré sú viditeľné ako svetlo.

Častice s energiou nad  $10^{20}$  eV vytvárajú atmosférickú spršku, ktorá sa rozkladá na častice, ktoré sú viditeľné ako svetlo. Častice s energiou nad  $10^{20}$  eV vytvárajú atmosférickú spršku, ktorá sa rozkladá na častice, ktoré sú viditeľné ako svetlo.

Častice s energiou nad  $10^{20}$  eV vytvárajú atmosférickú spršku, ktorá sa rozkladá na častice, ktoré sú viditeľné ako svetlo. Častice s energiou nad  $10^{20}$  eV vytvárajú atmosférickú spršku, ktorá sa rozkladá na častice, ktoré sú viditeľné ako svetlo.

Častice s energiou nad  $10^{20}$  eV vytvárajú atmosférickú spršku, ktorá sa rozkladá na častice, ktoré sú viditeľné ako svetlo. Častice s energiou nad  $10^{20}$  eV vytvárajú atmosférickú spršku, ktorá sa rozkladá na častice, ktoré sú viditeľné ako svetlo.

Častice s energiou nad  $10^{20}$  eV vytvárajú atmosférickú spršku, ktorá sa rozkladá na častice, ktoré sú viditeľné ako svetlo. Častice s energiou nad  $10^{20}$  eV vytvárajú atmosférickú spršku, ktorá sa rozkladá na častice, ktoré sú viditeľné ako svetlo.

Častice s energiou nad  $10^{20}$  eV vytvárajú atmosférickú spršku, ktorá sa rozkladá na častice, ktoré sú viditeľné ako svetlo. Častice s energiou nad  $10^{20}$  eV vytvárajú atmosférickú spršku, ktorá sa rozkladá na častice, ktoré sú viditeľné ako svetlo.

## Skok

Apertúra prevyšuje AGASA apertúru viac než 1000 krát

Na skúmanie unikálnych vysokoenergetických javov je potrebné rozšíriť apertúru na pozorovanie. Takýto inštitút pre Výskum kozmického žiarenia bol vytvorený "JEM-EUSO" v roku 2008. 700 km<sup>2</sup> v Utahu, USA, ako súčasť AGASA. Najväčšia sieť detektorov v súčasnosti, s rozlohou 3,500 km<sup>2</sup>, vznikla v roku 2005 v Argentíne, Observatórium Pampa Augusta (PAM). Pampa Augusta je mesto francúzskeho vesmáru, ktorý ako prvý objavil atmosférickú spršku nad 70 rokov. Pozemné observatóriá sú obmedzené pozorovaním buď svetovej alebo južnej polkryky, nedejúce obe strany. Pozemné detektory týchto nabitých častíc detektujú iba smerom na zem. Observatórium skúmajúce prenikajúce zeme, JEM-EUSO, má veľký úspech vo veľkosti pozorovanej oblasti, pokrývajúcej 100,000 - 300,000 km<sup>2</sup> (viac ako trikrát AGASA) málokedy pozorované vo výške 100 km na obežnej dráhe zeme. Pôvodná sieť AGASA mala tvar polkryky, ktorá mala polomer 60°. JEM-EUSO má tvar polkryky, ktorá mala polomer 60°. JEM-EUSO má tvar polkryky, ktorá mala polomer 60°.

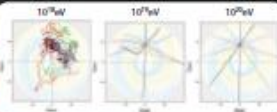


## Výzva

Očakávané výsledky vesmírneho teleskopu JEM-EUSO

### Astronómia nabitých častíc vo Vesmíre

Takže nabitých častíc rastie na Zemi, každú sekundu na každý  $m^2$ . So zvyšujúcou sa energiou častíc, ich traja klesá so zvyšovaním energie častíc. Odkiaľ sa, že prichádzajúca nabitá častica s energiou nad  $4 \times 10^{19}$  eV budú existovať? Generálna strata pri spozorovaní kozmických častíc s energiou nad  $10^{20}$  eV. Po objavení častíc s energiou  $10^{20}$  eV v roku 1962. Uskutočnením, ktoré nových častíc, a podrobným sledovaním boli spozorované v 90. rokoch v projektoch Akeno-Giant Air Shower Array (AGASA) na Univerzite v Tokyu a Tj/ Ene16-Res Experiment-om na Univerzite v Utahu. Pôvod vysokoenergetických častíc je neznámy a fascinujúci, a pokiaľ možno vedecky záujem.



1) Každá 10. sekunda nabitá častica s energiou nad  $10^{20}$  eV padá na Zem.

### Skúmanie vesmíru pri najvyššej energii

Nabitá častica dopadajúca na zemskú atmosféru sa rozkladá a vytvára atmosférickú spršku. Táto sprška sa rozkladá na častice, ktoré sú viditeľné ako svetlo. Častice s energiou nad  $10^{20}$  eV vytvárajú atmosférickú spršku, ktorá sa rozkladá na častice, ktoré sú viditeľné ako svetlo. Častice s energiou nad  $10^{20}$  eV vytvárajú atmosférickú spršku, ktorá sa rozkladá na častice, ktoré sú viditeľné ako svetlo.

### Enerygetická hranica - prevyšujúca LHC fyziku

Nabitá častica dopadajúca na zemskú atmosféru sa rozkladá a vytvára atmosférickú spršku. Táto sprška sa rozkladá na častice, ktoré sú viditeľné ako svetlo. Častice s energiou nad  $10^{20}$  eV vytvárajú atmosférickú spršku, ktorá sa rozkladá na častice, ktoré sú viditeľné ako svetlo. Častice s energiou nad  $10^{20}$  eV vytvárajú atmosférickú spršku, ktorá sa rozkladá na častice, ktoré sú viditeľné ako svetlo.

### Monitorovanie atmosférického osvetlenia z celej Zeme

Nabitá častica dopadajúca na zemskú atmosféru sa rozkladá a vytvára atmosférickú spršku. Táto sprška sa rozkladá na častice, ktoré sú viditeľné ako svetlo. Častice s energiou nad  $10^{20}$  eV vytvárajú atmosférickú spršku, ktorá sa rozkladá na častice, ktoré sú viditeľné ako svetlo. Častice s energiou nad  $10^{20}$  eV vytvárajú atmosférickú spršku, ktorá sa rozkladá na častice, ktoré sú viditeľné ako svetlo.

# JEM-EUSO na Medzinárodnej Vesmírnej Stanici

## skúma pôvod vysokoenergetických častíc vo Vesmíre.

1) Každá 10. sekunda nabitá častica s energiou nad  $10^{20}$  eV padá na Zem.





# JEM-EUSO

## Flight Segment

TDRS

EECR

HTV

UV photons

Fluorescence

Cherenkov

Air Shower

H-IIB

Ground Support Equipment

Ground Segment

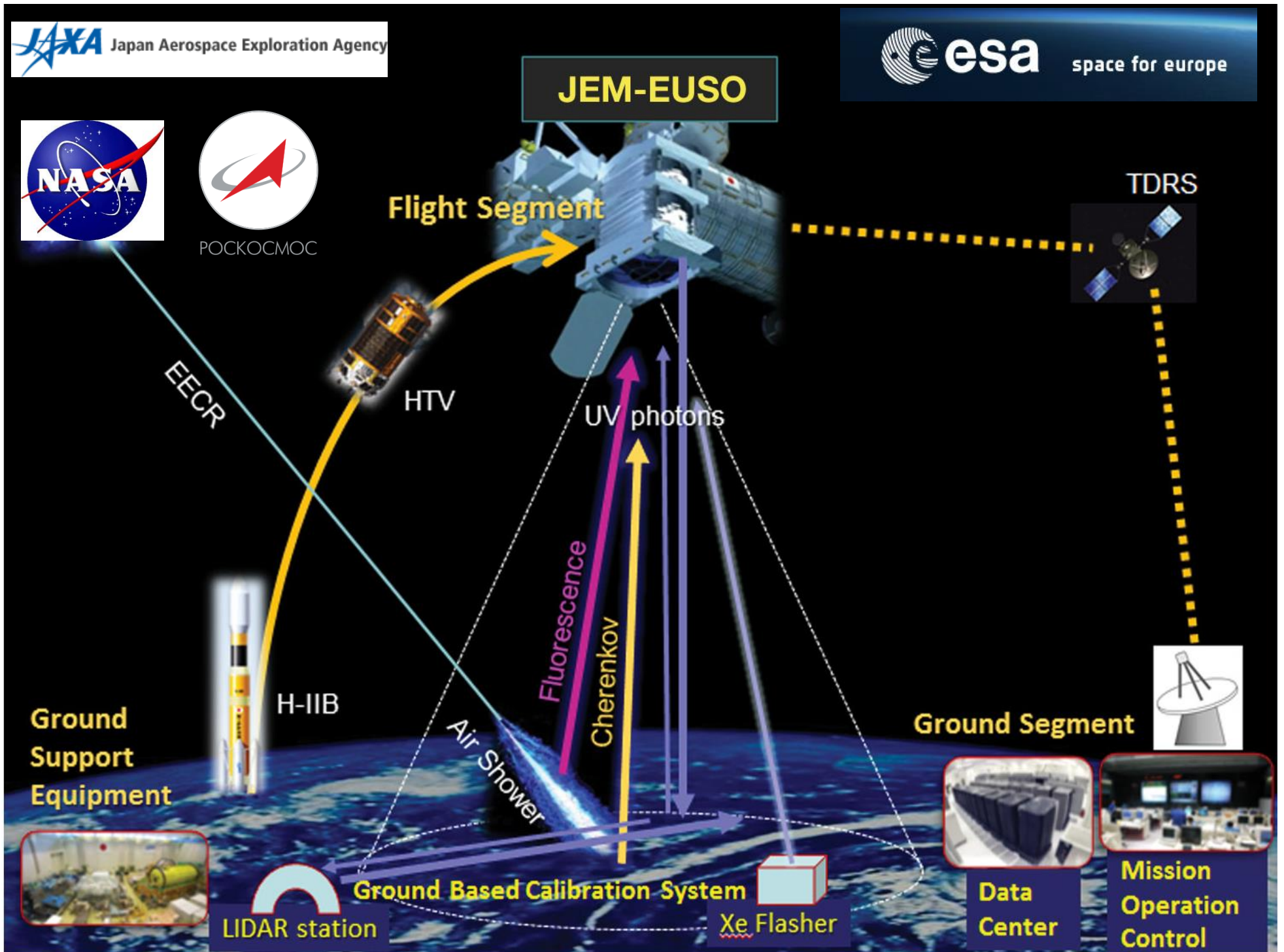
Ground Based Calibration System

Xe Flasher

LIDAR station

Data Center

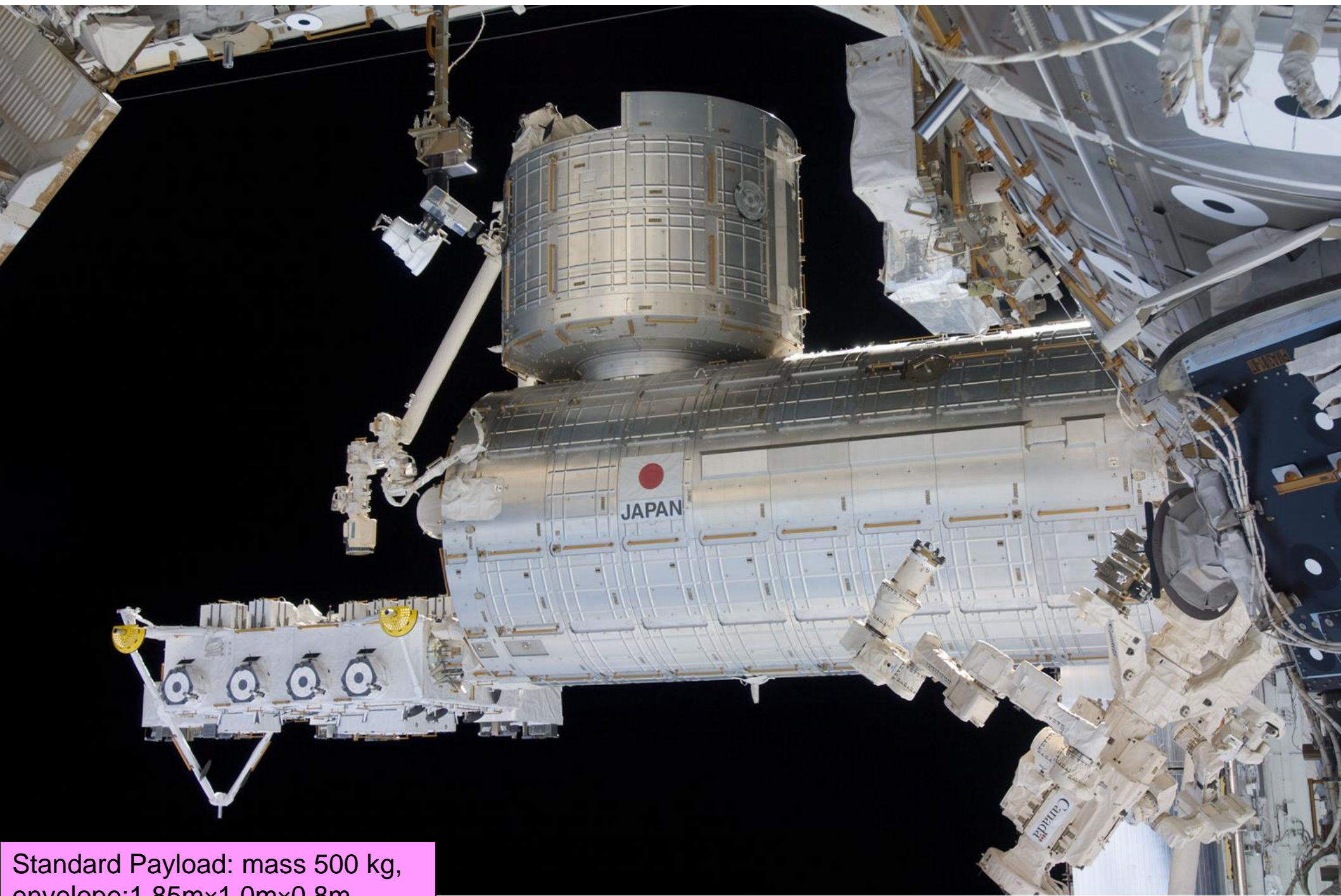
Mission Operation Control



## ***JEM-EUSO mission main parameters***

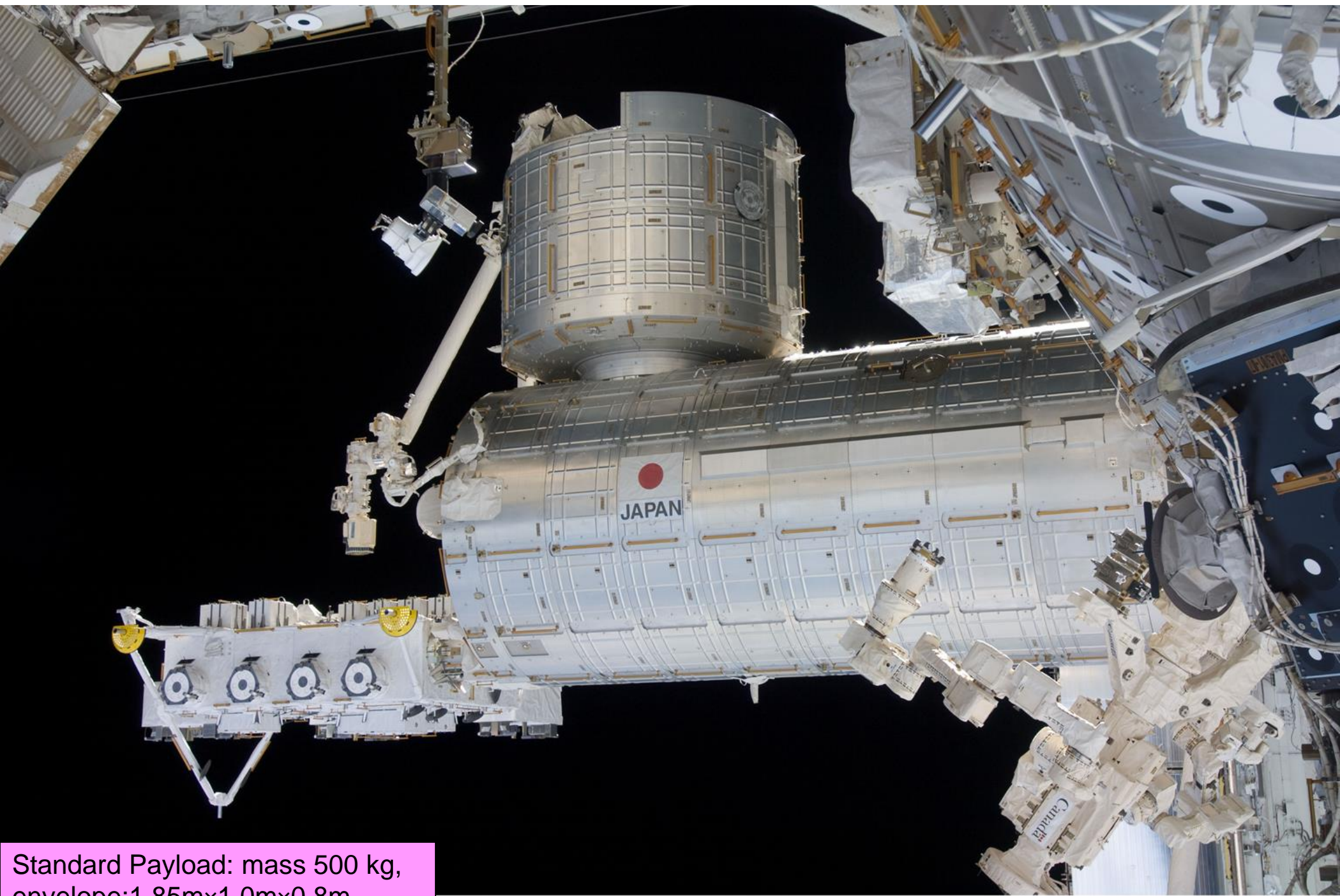
<b>Parameter</b>	<b>Value</b>
<b>Launch date</b>	<b>JFY 2016</b>
<b>Mission Lifetime</b>	<b>3+2 years</b>
<b>Rocket</b>	<b>H2B</b>
<b>Transport Vehicle</b>	<b>HTV</b>
<b>Accommodation on JEM</b>	<b>EF#2</b>
<b>Mass</b>	<b>1938 kg</b>
<b>Power</b>	<b>926 W (op.) 352 W (non op.)</b>
<b>Data rate</b>	<b>285 kbps (+ on board storage)</b>
<b>Orbit</b>	<b>400 km</b>
<b>Inclination of the Orbit</b>	<b>51.6°</b>
<b>Operation Temperature</b>	<b>-10° to 50°</b>





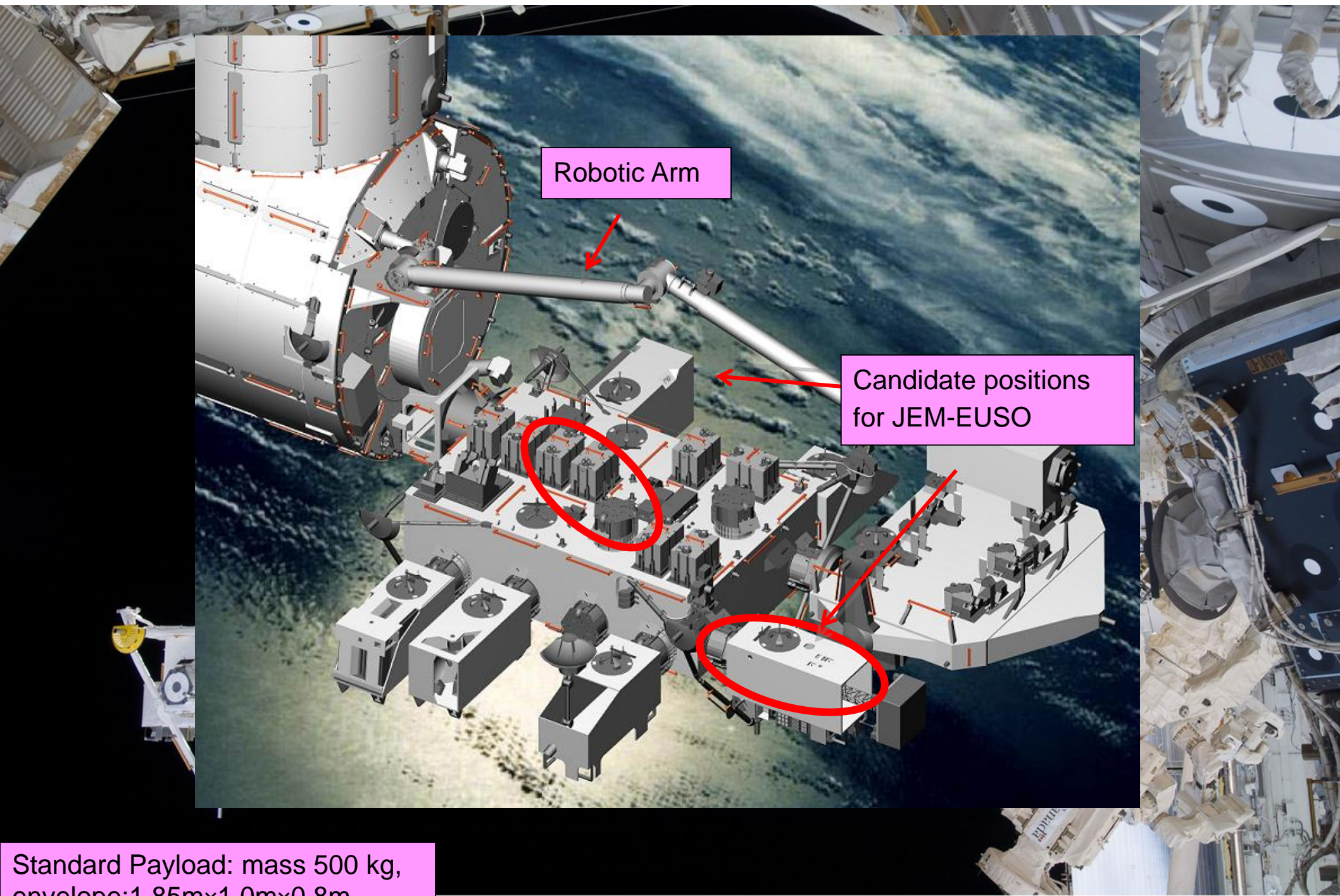
Standard Payload: mass 500 kg,  
envelope: 1.85m×1.0m×0.8m





Standard Payload: mass 500 kg,  
envelope: 1.85m×1.0m×0.8m





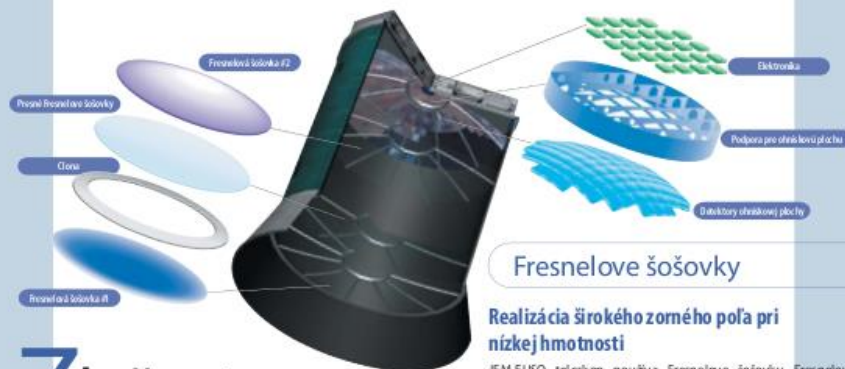
Robotic Arm

Candidate positions  
for JEM-EUSO

Standard Payload: mass 500 kg,  
envelope: 1.85m×1.0m×0.8m



# Najnovšie Technológie v službách JEM-EUSO



## Fresnelove šošovky

### Realizácia širokého zorného poľa pri nízkej hmotnosti

JEM-EUSO teleskop používa Fresnelove šošovky. Fresnelova šošovka je poloplochá šošovka, ktorá má kruhové drážky, ktoré eliminujú veľkú hmotnosť štandardných konvexných a konkávných šošoviek. Tenkosť a ľahkosť Fresnelovej šošovky je nevyhnutnou podmienkou jej využitia vo vesmíre, pričom ponúka rovnaké optické funkcie ako hrubé a ťažké šošovky. JEM-EUSO používa dve zakrivené obojstranné Fresnelove šošovky z UV priepustného plastu a jednu mikrometrickú Fresnelovu šošovku. Tento dizajn umožňuje najvyššiu účinnosť širokého zorného poľa. Veľkosť trojitej šošovky je 2,5 m v priemere, zložený zo stredovej 1,5 m časti a kruhového povrchu prstencových šošoviek.

## Zloženie

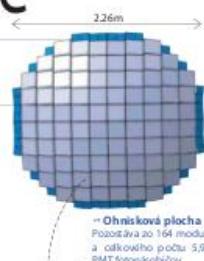
### Detektory ohniskovej plochy

#### 6,000 fotonásobičov

Ohnisková plocha je zakrivená s priemerom 2,26 m. 6000 1-palcových štvorcových multianódových rúriek fotonásobičov (PMTs) detektuje svetlo z rôznych miest v zemské atmosfére. Predchádzajúce fotonásobiče (PMTs) mali obmedzenú fotosenzitívnu plochu približne 45%. JEM-EUSO a Hamamatsu Photonics spoločne vyvinuli fotonásobiče (PMTs), ktoré majú účinnú plochu 85%.



85% povrchu PMT fotonásobičov tvorí aktívna plocha, majúca 6 x 6 pixelov s celkovou plochou 36,2 mm štvorcových.

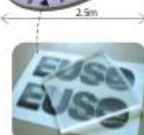


Svetlotvorný modul pokrýva ohniskovú plochu s priemerom 2,26 m s 5,964 PMT fotonásobičmi, z ktorých má každý 6 x 6 = 36 svetlotvorných jednotiek.

## Vypustenie

### Transportný dopravník agentúry JAXA pre kozmickú stanicu (HTV) nesie JEM-EUSO

HTV bude vypustený H-IIIB raketou (JAXA) ktorá preniesie JEM-EUSO k ISS. Robotické ramená na ISS umiestnia JEM-EUSO na JEM modul "Kibo".



Konfigurácia stredovej šošovky a priestoru ových šošoviek umožňuje vyvinúť šošovku veľkosti modulu byť vyvinutá na jednom stroji.



Transportný dopravník kozmickej stanice (HTV) pletá k ISS, JAXA

## Porovnanie JEM-EUSO s najväčšími pozemnými observatóriami

	AGASA	HiRes	Auger	Telescope Array	JEM-EUSO
Organizácia	Tókijská Univerzita	Univerzita v Utahu	Medzinárodné konzorcium	Tókijská Univerzita a Univerzita v Utahu	Medzinárodné konzorcium
Miesto	Yamanashi, Japonsko	Utah, USA	Argentína	Utah, USA	Medzinárodná vesmírna stanica
Typ detektorov	Pozemná sieť	Fluorescenčný pozemný teleskop	Pozemná sieť + Fluorescenčný pozemný teleskop	Pozemná sieť + Fluorescenčný pozemný teleskop	Fluorescenčný vesmírny teleskop
Doba prevádzky	1990–2004	1997–2006	2005–	2007–	Vypustenie očakávané v 2013
Efektívna apertúra (km <sup>2</sup> )	150	500	~7,000	760	125,000
Výskyt EHE udalostí (počet/rok)	1, experimenty ukončené	Menej ako 1 experimenty ukončené	50 (očakávané), 3 (pozorované)	10 (očakávané)	350 – 1,700 (očakávané)

## JEM-EUSO misia

Výška	okolo 400km	Počet pixelov ohniskového povrchu	okolo 0.2 miliónov
Pozorovacia dĺžka a šírka	N51°–55°1' x všetky dĺžky	Rozlíšenie na zemi	okolo 0.8 km
Zorné pole	60°	Strieda	12–25%
Apertúra (pozemná plocha)	0.2 miliónov km <sup>2</sup>	Trvanie misie	3 (+2) rokov
Priemer teleskopu	2.5 m	Celková hmotnosť	~1.9 ton
Optický systém	Dve zakrivené obojstranné Fresnelove šošovky a vysokopriehľadná Fresnelova šošovka	Prikon	< 1kW

## Medzinárodní Partneri

	Japonsko	RIKEN, Konan Univ., Fukui Tech. Univ., Aoyama Gakuin Univ., Saitama Univ., NIRS, Univ. Tokyo, Tohoku Univ., ICRR, Univ. Tokyo, KEK, Chiba Univ., NAOJ, ISAS/JAXA, Kanazawa Univ., Nagoya Univ., STE Lab., Nagoya Univ., Yukawa Inst., Kyoto Univ., Kyoto Univ., Kobe Univ., Kinki Univ., Hiroshima Univ., Hokkaido Univ., Tokyo Inst. Tech.
	USA	NASA/MSFC, UAH, LBL, UCB, UCLA, Vanderbilt Univ., Univ. Arizona.
	Francúzsko	APC-Paris 7, LAL, IN2P3-CNRS
	Nemecko	MPI Munich, Univ. Tuebingen, MPI Bonn, Univ. Erlangen, LMU&MPQ
	Taliansko	Univ. Florence, Univ. Naples, Univ. Palermo, Univ. Rome "Tor Vergata", Univ. Turin, INdA/CNR, IASF-PA/INAF, IFS-TO/INAF, INFN
	Mexiko	ICN-UNAM, BUAP, UMSNH
	Kórejska republika	Ehwa W. Univ., Yonsei Univ.
	Rusko	SINP MSU, Dubna JINR
	Švajčiarsko	Neuchatel, CSEM, IACETH
	Španielsko	Univ. Alcalá
	Poľsko	IPJ, Podlasie Univ., Kielce Univ., Jagiellonian Univ.
	Slovensko	Inst. Experimentálnej fyziky, Košice

## Spolupáca JEM-EUSO

**Japonsko**  
Computational Astrophysics Laboratory, RIKEN  
2-1 Hirotsawa, Wako, Saitama 351-0198 Japan  
Tel.: +81-48-467-9417 Fax: +81-48-467-4078  
E-mail: jem-euso-staff@riken.jp URL: http://jemuso.riken.jp/

**Slovensko**  
Ústav Experimentálnej fyziky, Košice  
Watsonova 47, 040 01 Košice, Slovensko  
Tel.: +421 55 622 45 54 Fax: +421 55 633 62 92  
E-mail: jem-euso@sfk.kosice.sk URL: http://space.ssfk.sk/

# *Main Objective: Astronomy and Astrophysics through the particle channel*

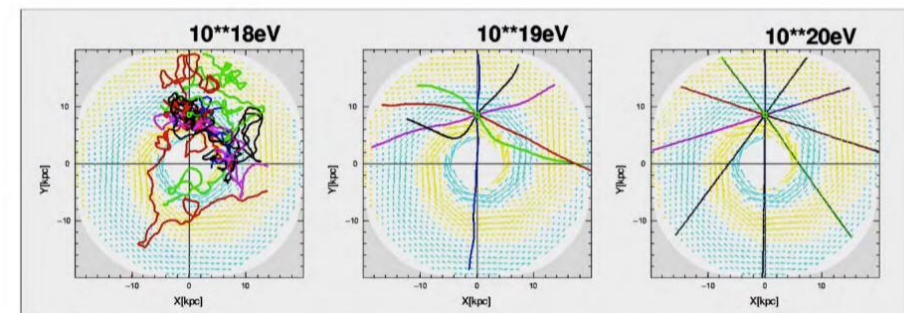
## Main Scientific Objectives

- *Identification of sources by high-statistics arrival direction analysis (+multi-wavelength!)*
- *Measurement of the energy spectra of individual sources (spectral shape, flux, power)*



Physics and Astrophysics  
at  $> 5. \times 10^{19}$  eV

Galactic-MF structure & UHECR propagation



# *Exploratory Scientific Objectives*

## *Exploratory Objectives: new messengers*

- ***Discovery of UHE neutrinos*** by neutrino discrimination and identification via  $X_0$  and  $X_{max}$
- ***Discovery of UHE Gammas***

## *Exploratory Objectives: magnetic fields*

- ***Constrains on the galactic and local extragalactic fields***

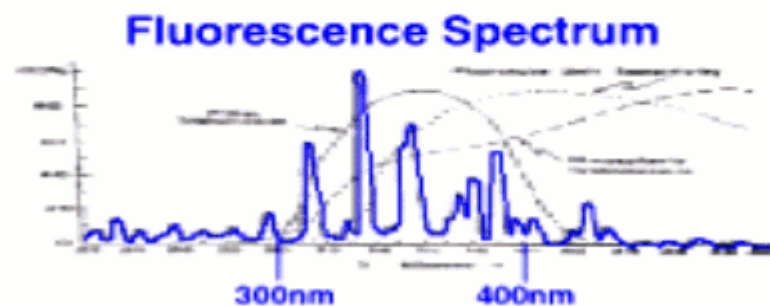
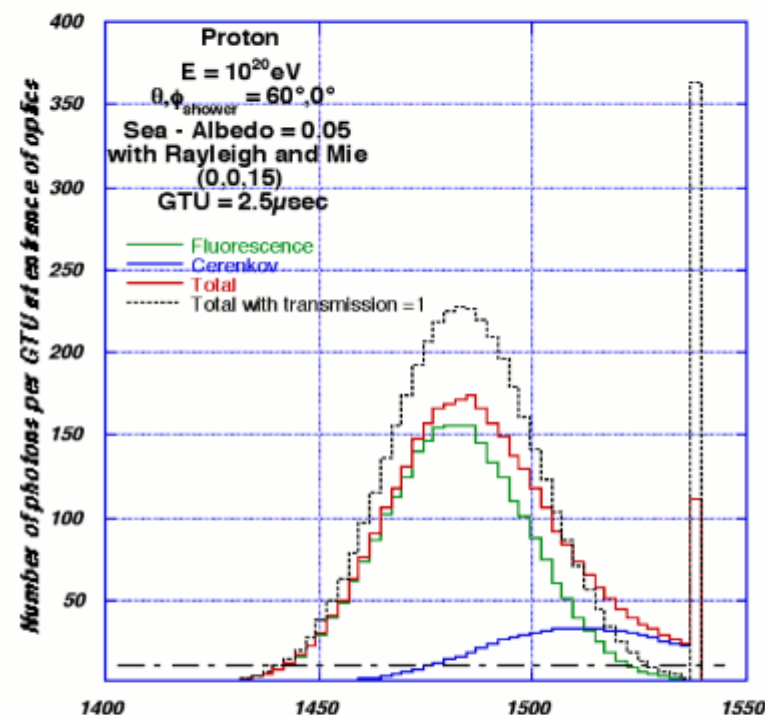
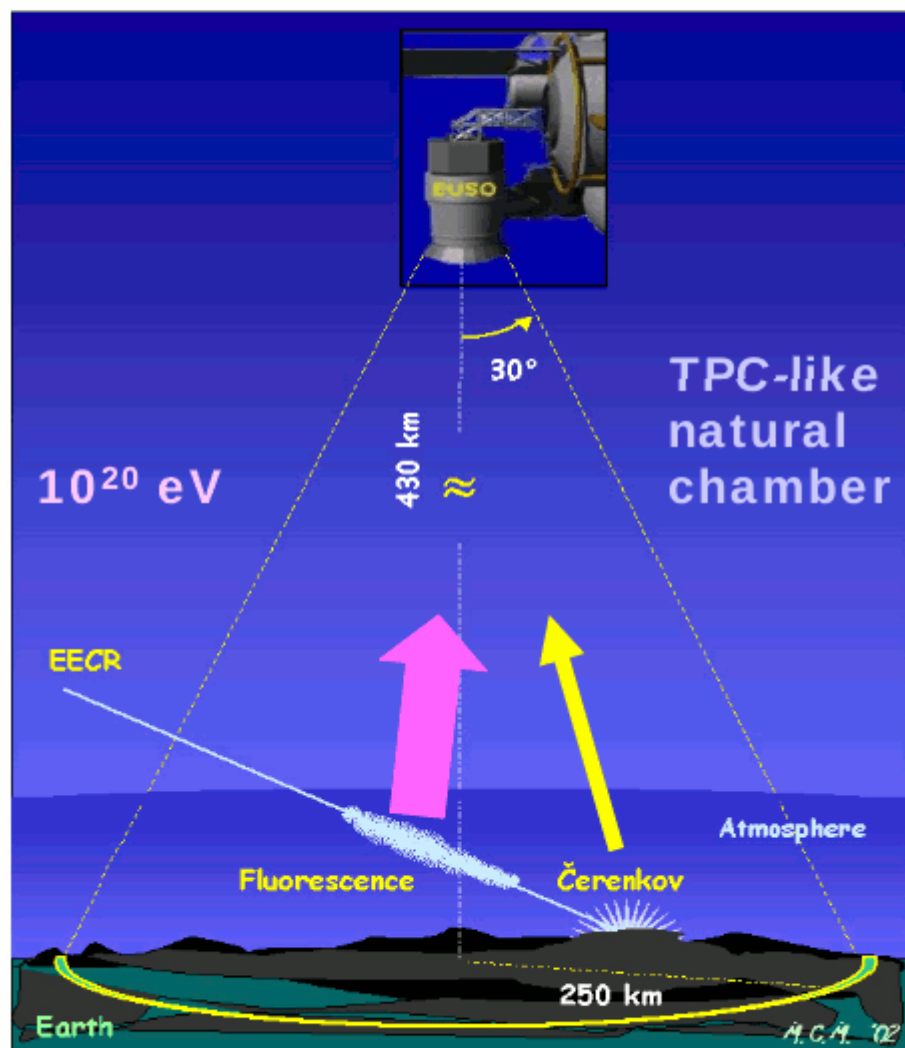
## *Exploratory Objectives: Atmospheric science*

- ***Nightglow***
- ***Transient luminous events***



# Principle of EUSO

- first *remote-sensing* from space, opening a new window for the highest energy regime

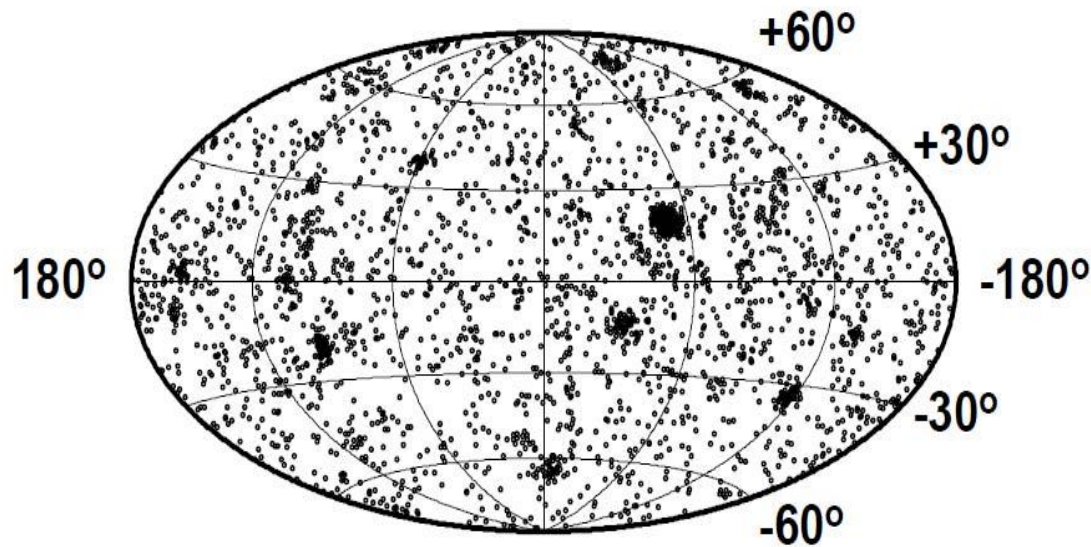


Cf: Ground-based arrays < 0.01 EUSO

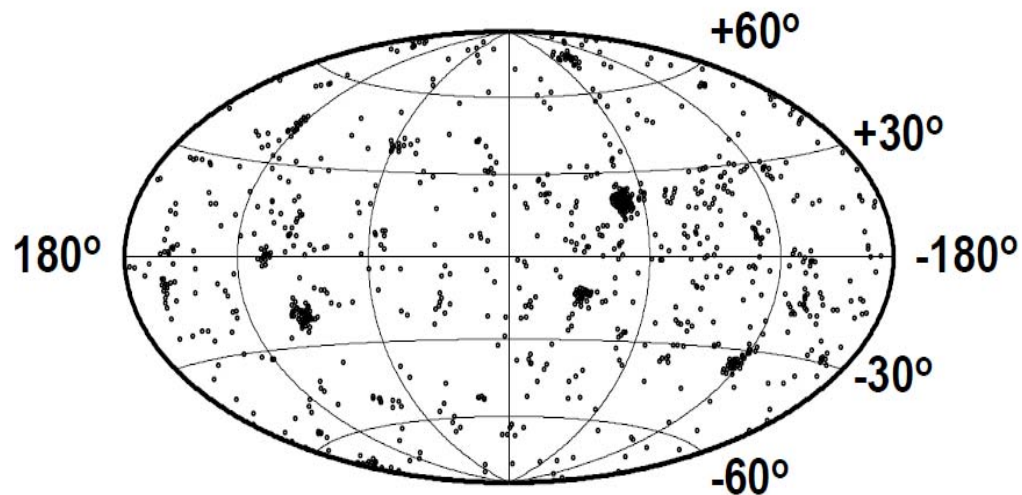
(1) Scintillator array, (2) Fluorescence telescope array

From College de France: better data now

## Simulation assuming that UHECR sources are AGN



**3000 events**  
 **$E > 5 \cdot 10^{19} \text{eV}$**



**1000 events**  
 **$E > 7 \cdot 10^{19} \text{eV}$**

# EUSO precursor experiments

*Series of precursor  
EUSO experiments to  
improve and show TRL  
of „state of art“ EUSO  
class detectors*

*Show readiness of  
collaboration to build  
main detector*

**TA-EUSO (2015)**

**EUSO balloon (2014)**

**EUSO-SPB (2017)**

**Mini-EUSO (2018)**

**EUSO-SPB 2 (2020+)**

**K-EUSO (2020+)**

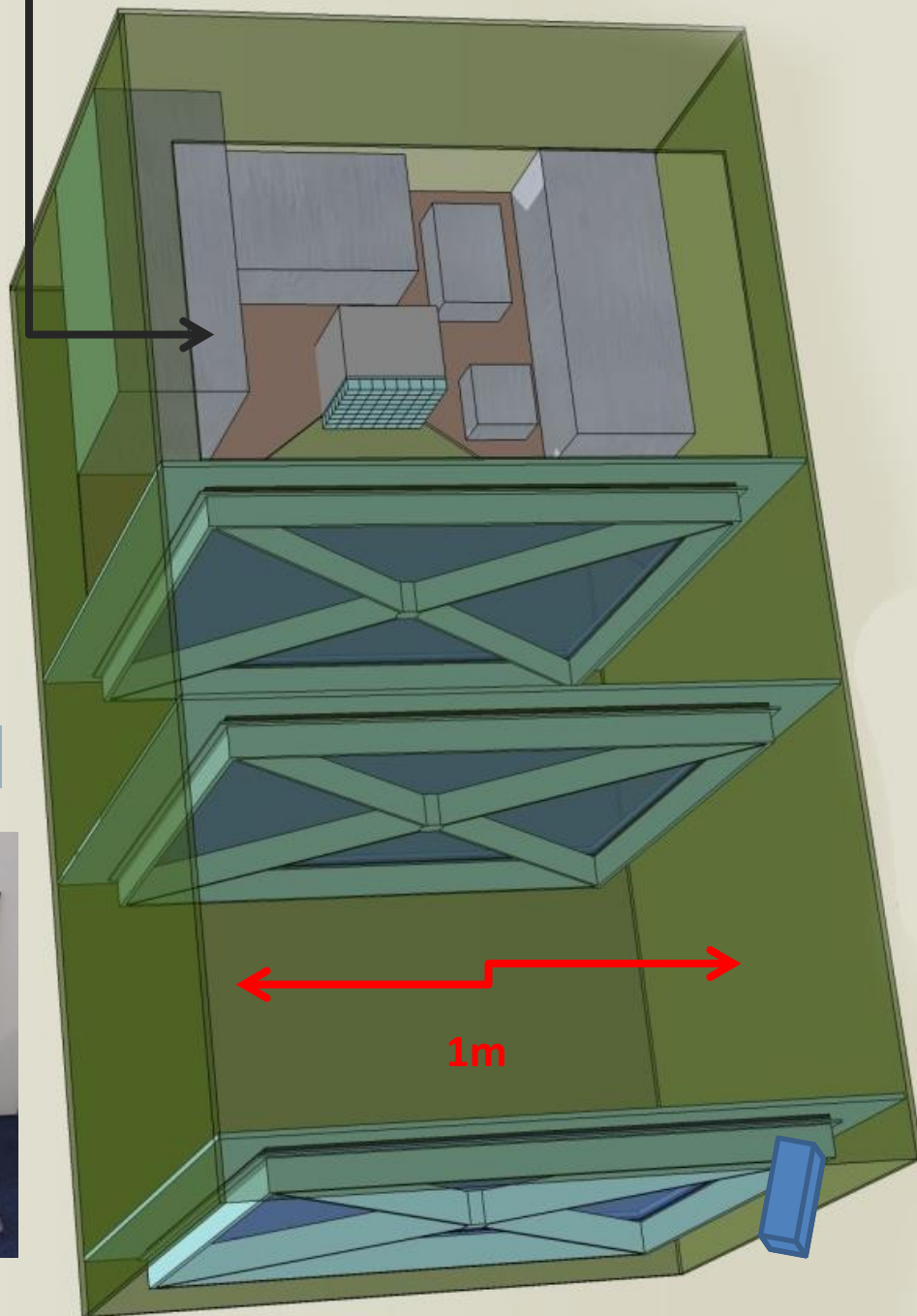


Electronics of detector

**EUSO  
balloon**

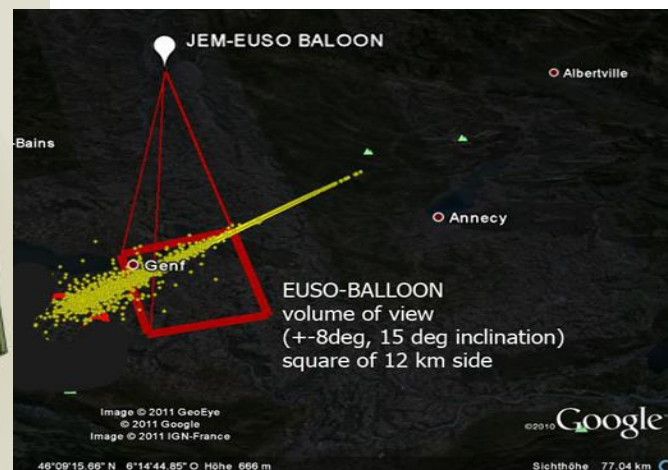
**august  
2014**

Lenses



## First JEM-EUSO precursor experiment

- lenses 1 m<sup>2</sup>
- 1 PMD
- ~300 kg
- waterproof gondola
- flight altitude ~38 km



Simulations



moving into the CU hall at Timmins 12.8.2014!



flight configuration : 18.8.2014





Timmins Stratospheric Balloon Base  
CNES - Canadian Space Agency  
24.-25. august 2014

~90 GB of data

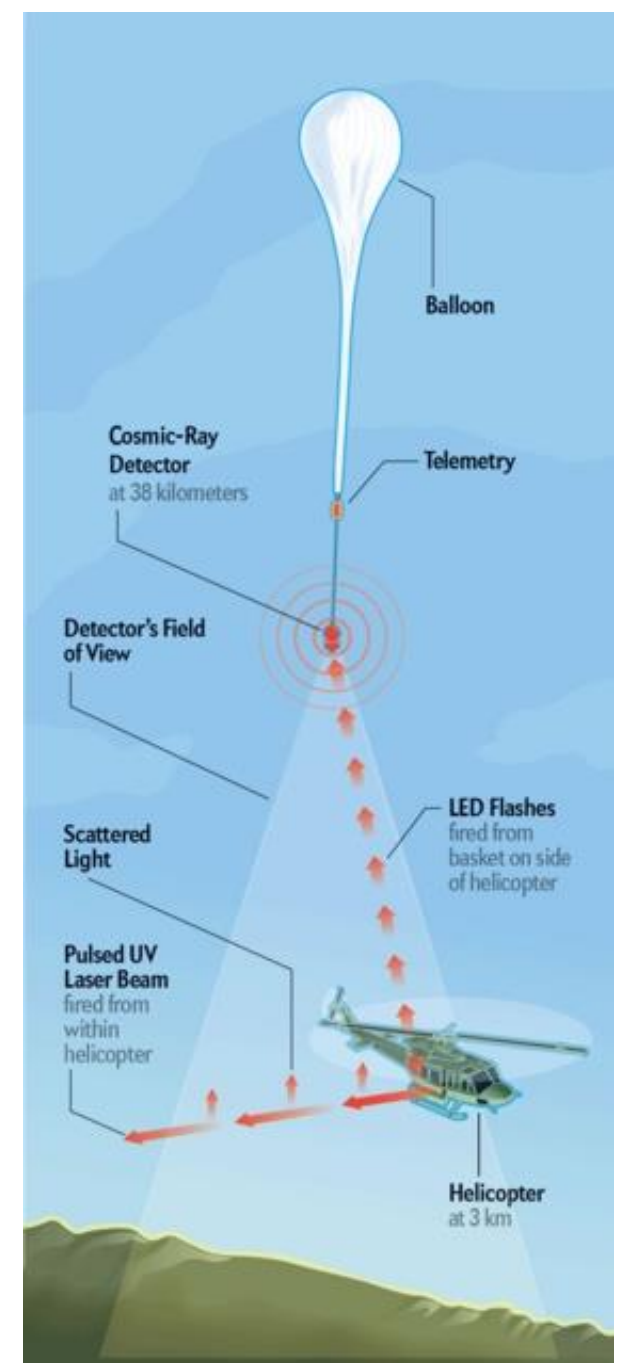
Start



gondola in hangar

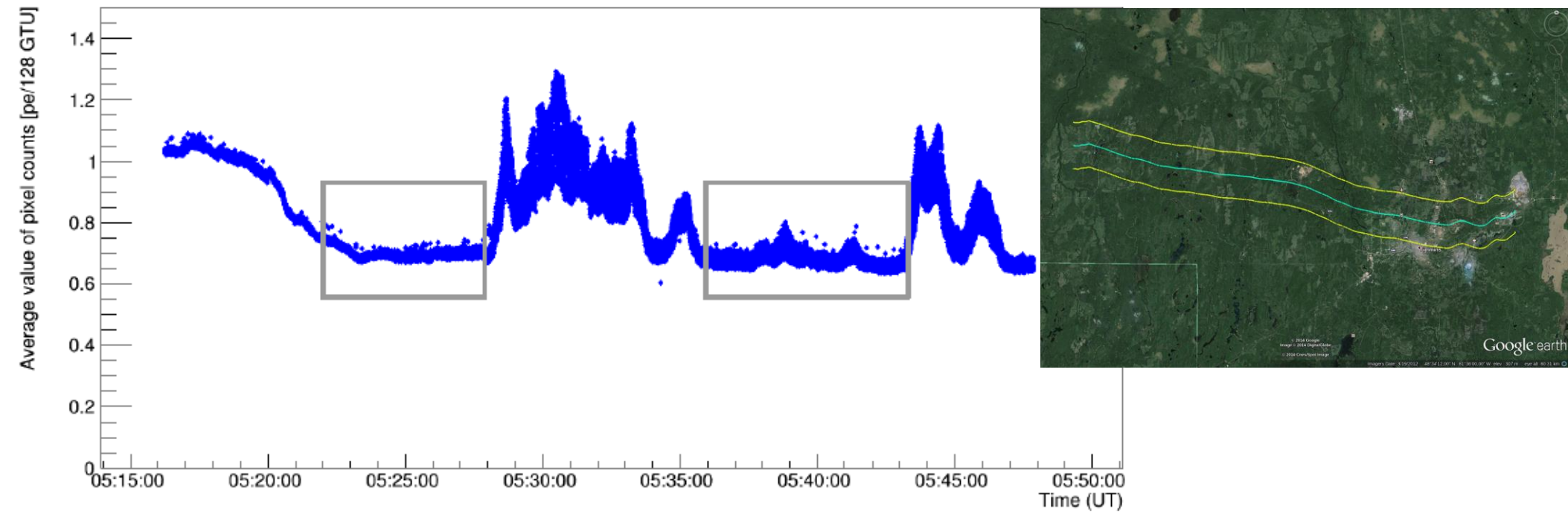


Landing in lake

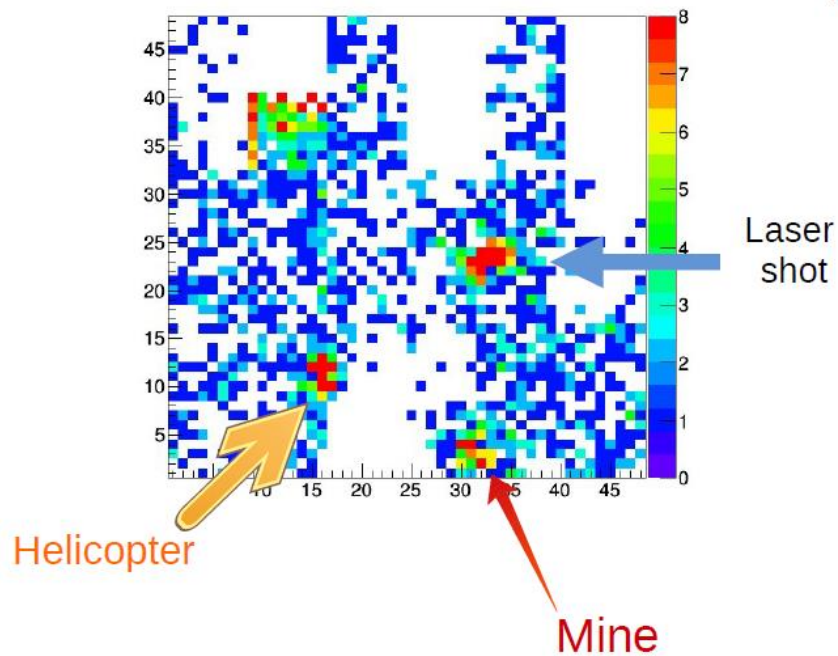


Scientific American article:  
Cosmic-Ray Telescope Flies High

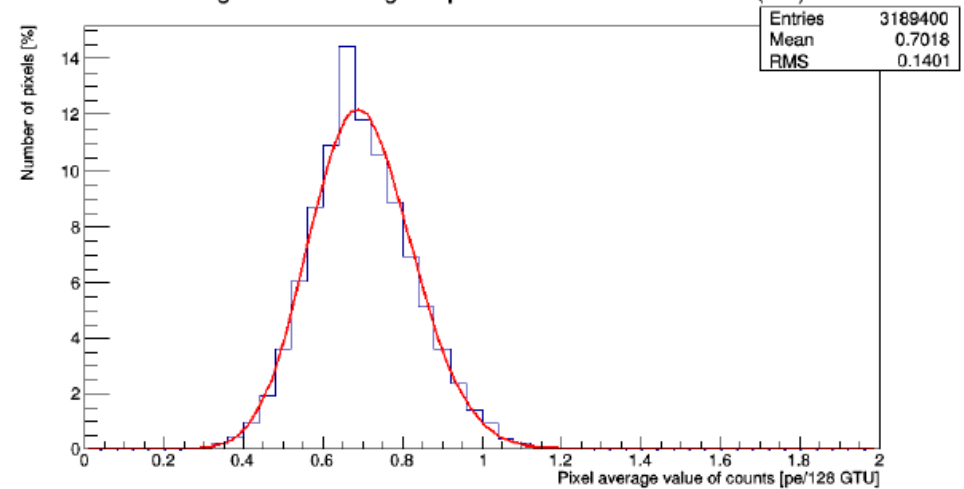
# EUSO-Balloon measurements



DAT: 05:33:52, Packet: 472, GTU: 007 → 05:34:24 (UT)



Histogram of active good pixels: 05:21:56 - 05:27:53 (UT)



Fitted by Poisson distribution  
with  $\lambda = 0.699$



# EUSO-TA

Start of measurements: 2015

Black Rock Mesa, Utah, at place of Telescope Array experiment

Hardware and software development, calibration, UV background observations at high zenith angles

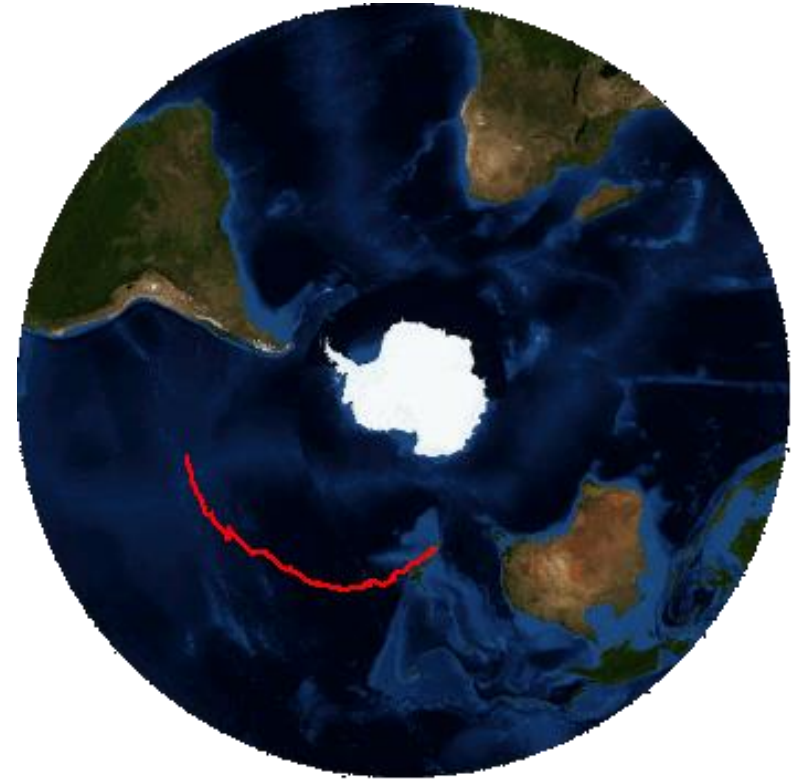




# EUSO precursor experiments

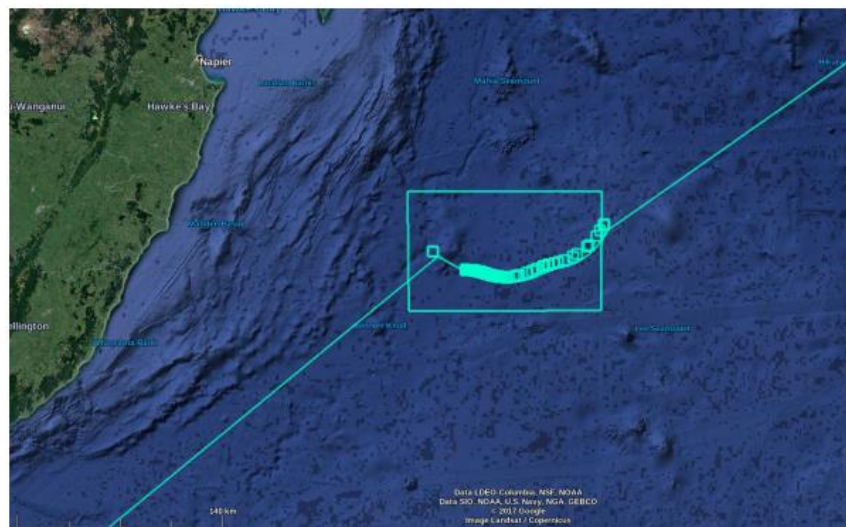
## EUSO-SPB NASA balloon

- start 24. april 2017 from Wanaka base
- expected flight duration 50 days, attempt to have record 100 days long flight
- first observation of shower from up
- balloon fall down after 12 days, reason not yet found/known
- detector work till the last moment

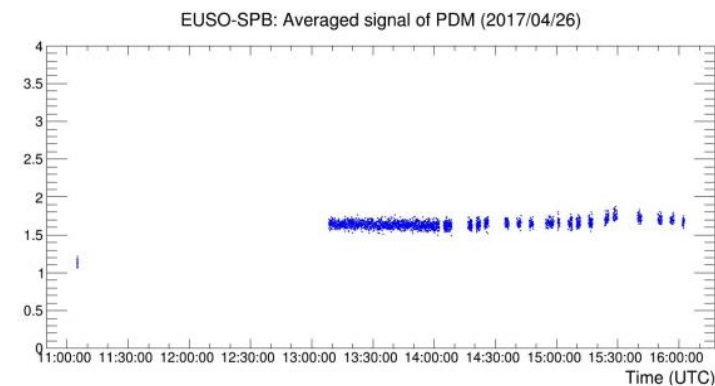
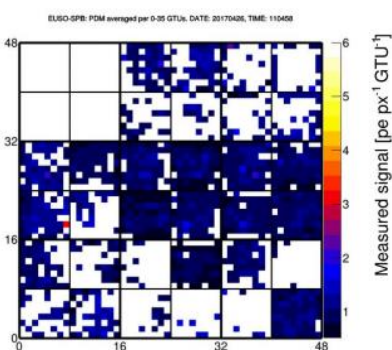
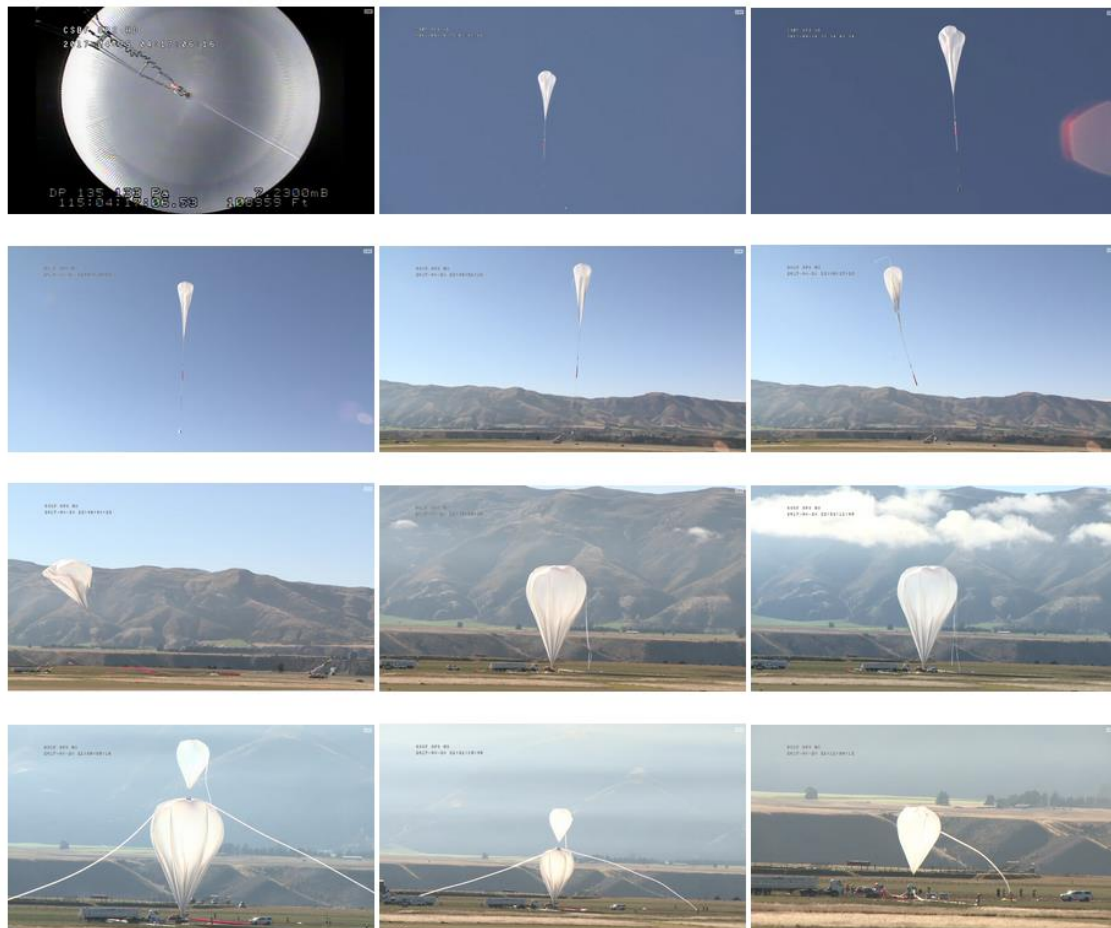
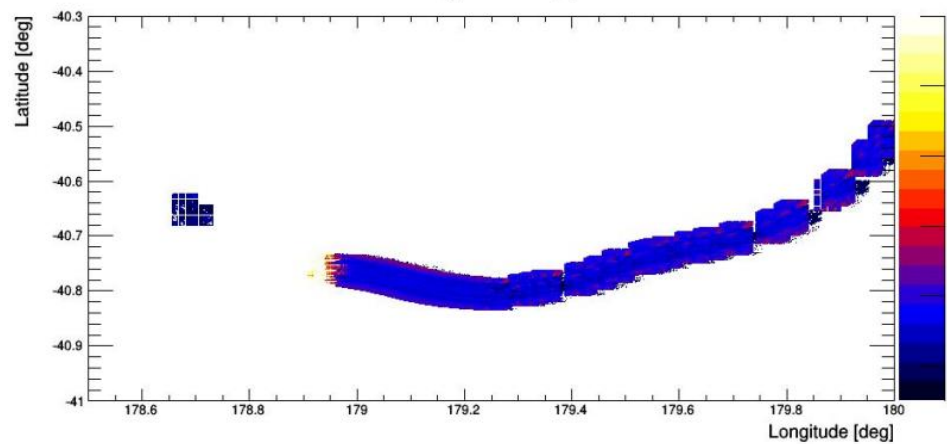


# EUSO – SPB1

Next start 2020+



EUSO-SPB: UV background map, DATE: 20170426





# Mini-EUSO

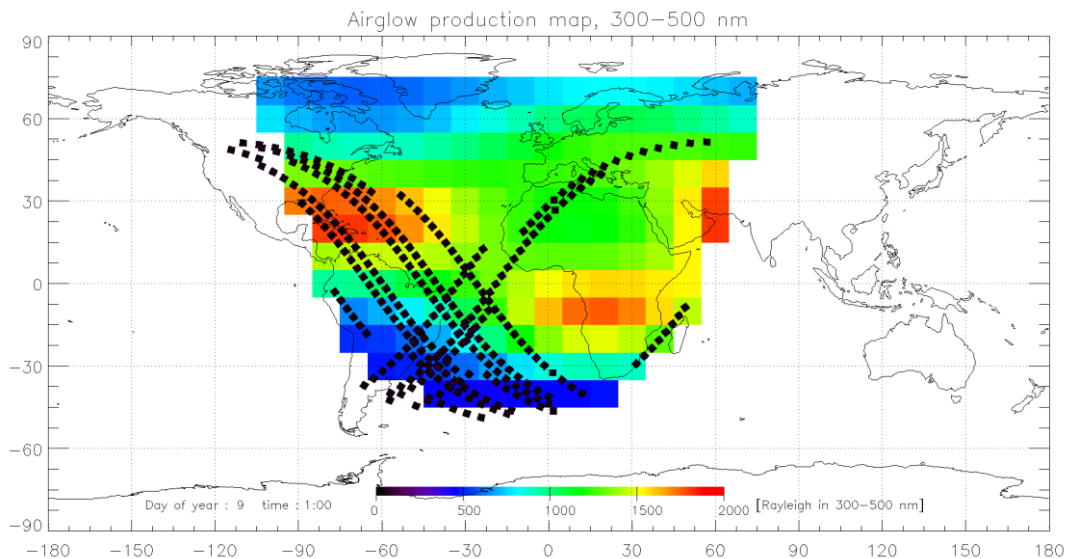
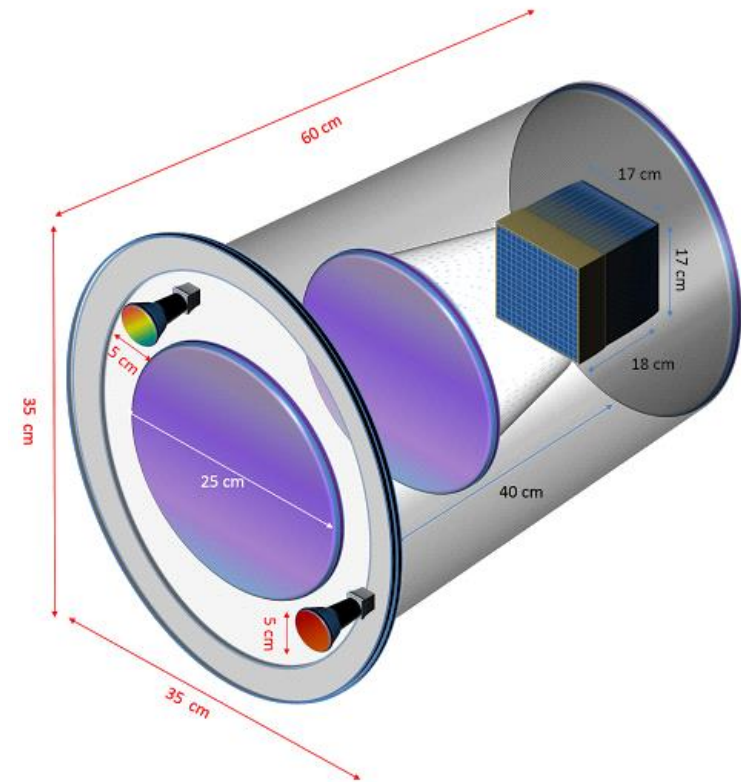
Start: end of year 2018

Located in one of two UV transparent windows in ISS

Weight: ~30 kg

Observations of

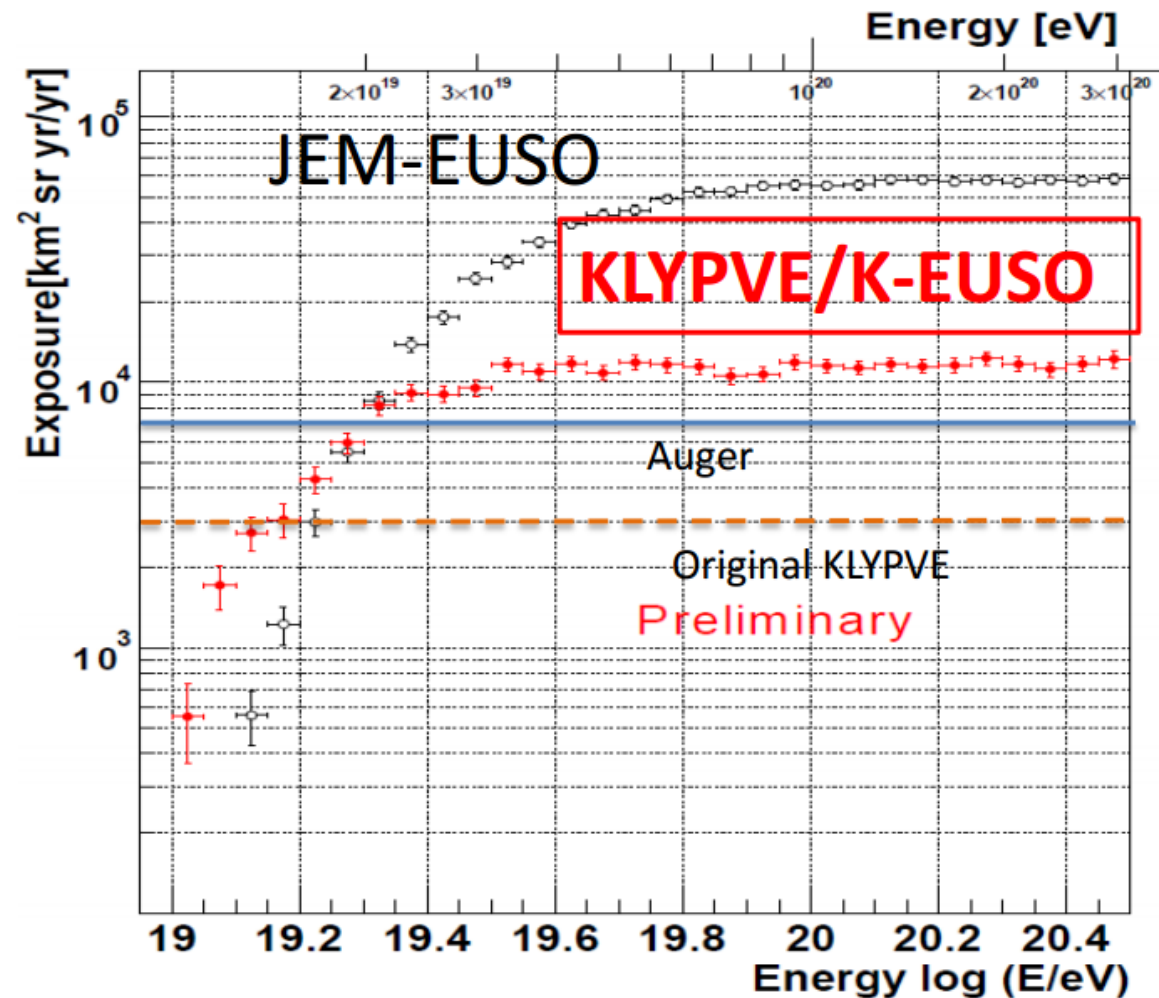
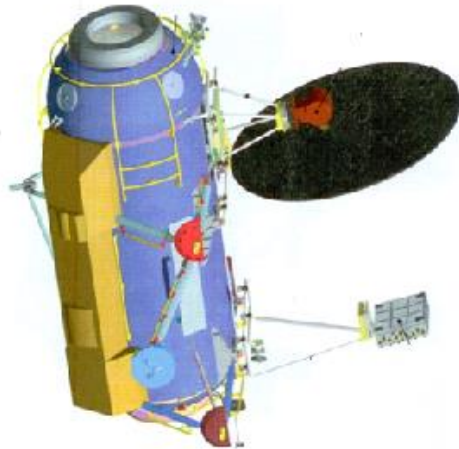
- UV background, TLE, bioluminescence



# K-EUSO



- KLYPVE projekt
- Start: 2020+
- Measurements from ISS
- 2020-2024 (2026)
- Concept based on mirror (10 m<sup>2</sup>)

One year exposition  $\sim 1.2 \times 10^4 \text{ km}^2 \text{ sr yr/yr}$  ( $\sim 1.7 \times$  more than Auger)  
r/yr)



N.Sakaki, F. Fenu et al.  
(ICRC2015 #647)

## 2013 : NASA Astrophysics in the Next Three Decades

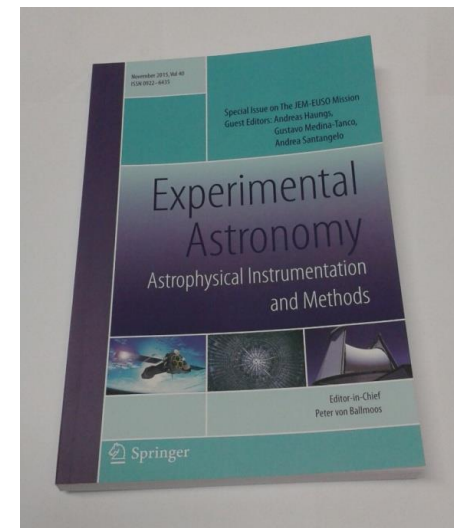
	Near-Term	Formative	Visionary
Gravitational Waves		 Gravitational Wave Surveyor	 Gravitational Wave Mapper
Cosmic rays	 JEM-EUSO		
Radio			 Cosmic Dawn Mapper
Microwaves		 CMB Polarization Surveyor	
Infrared	 JWST	 Far IR Surveyor	
Optical	 WFIRST-AFTA	 LUVOIR Surveyor	 ExoEarth Mapper
Ultraviolet	 TESS	 Gaia	
X-rays	 NICER	 Astro-H	
Gamma rays		 Xray Surveyor	 Black Hole Mapper

**Science**, *Catching cosmic rays where they live*, 7. august 2015, vol. 349, 6248

„Another ISS detector, the *Extreme Universe Space Observatory at the Japanese Experiment Module (JEM-EUSO)* - now being considered for launch in 2021 - would look down on Earth with a wide-angle camera, watching for ultraviolet light produced by the showers of particles that ultrahigh-energy cosmic rays spawn when they hit the atmosphere.“

### Selected JEM-EUSO overview

- 15 papers in special issue about JEM-EUSO experiment in journal *Experimental Astronomy*, Volume 40, Issue 1, 2015 (IF 1,99)



# Slovak participation in EUSO

Slovakia member since 2008, main research topics

## 1. UV background studies

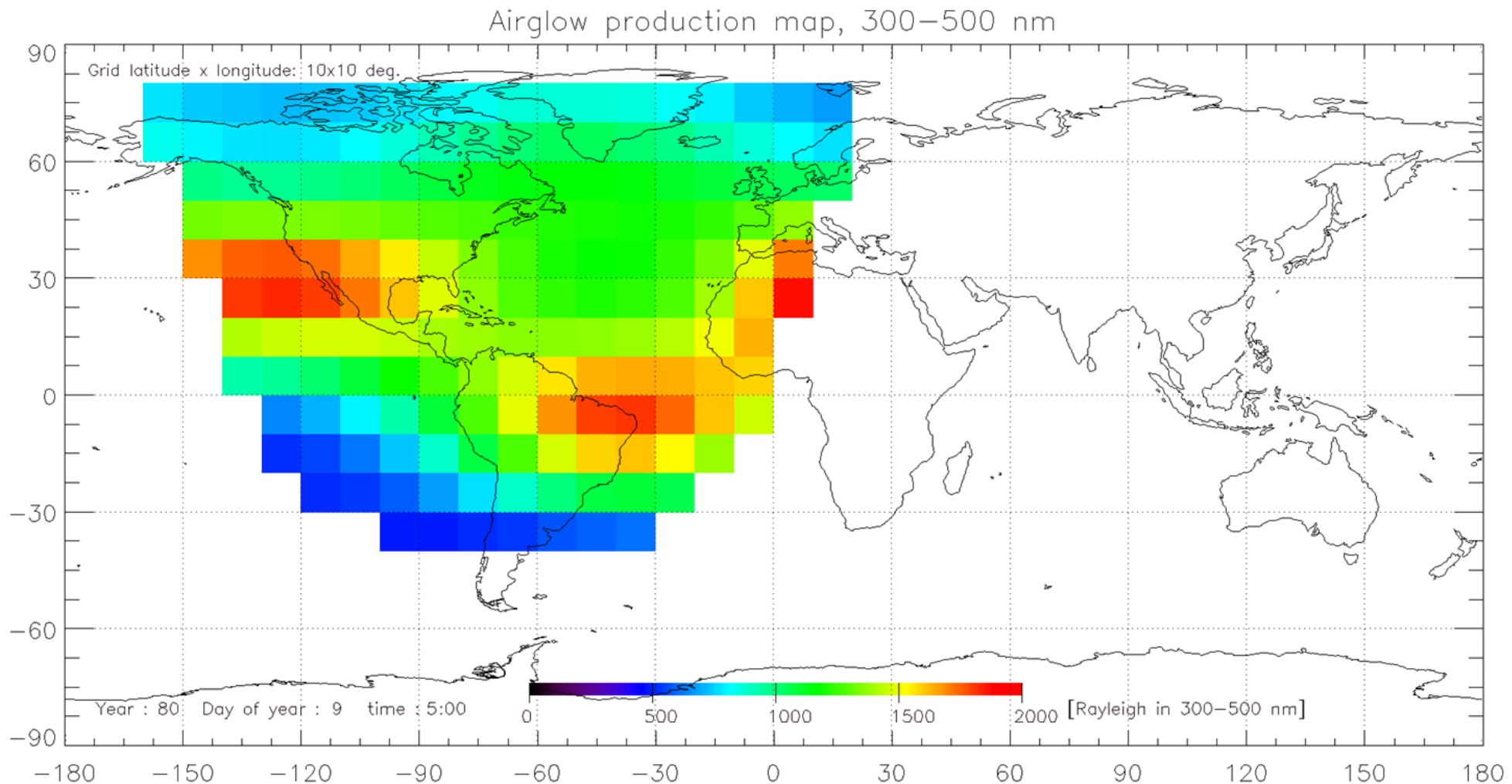
- UV background model development
- UV background analysis of EUSO experiments
- UV background measurements by AMON-net network

## 2. Pattern recognition of EAS

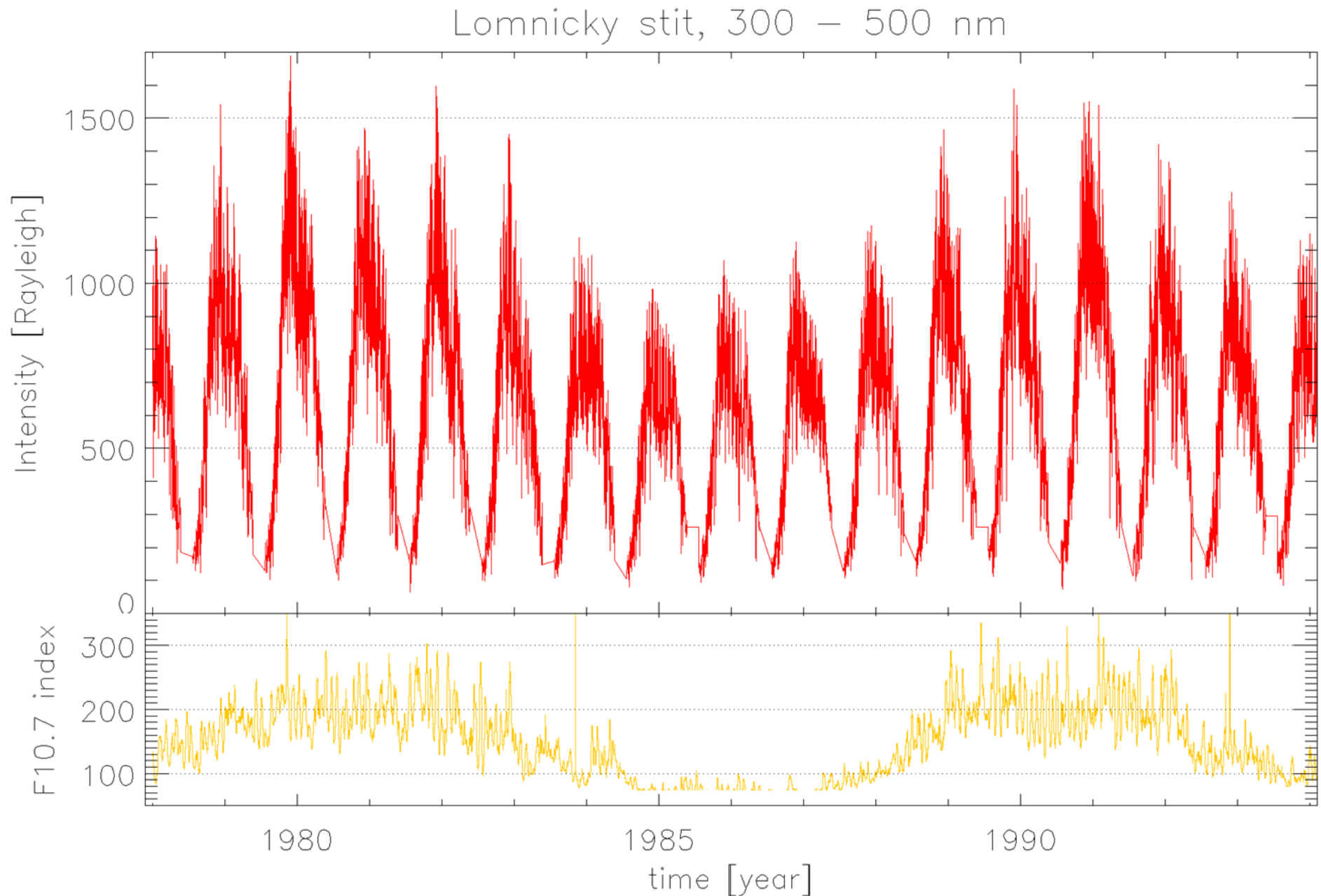


# UV background model development

- From models of light sources at the Earth's night side and radiation transfer model



# UV background model development



# Duty cycle estimation

## UV light sources

If background 1500 ph/(m<sup>2</sup> ns sr) is allowed [in % of total time on orbit]

- sun
- moon

} ~ 21-22 %

- airglow/nightglow
- zodiacal light
- integrated faint star light

} ~ 20-21%

- Boreal/austral auroras ~ 1%

- South Atlantic anomaly small

- Lightning and TLEs ~ 2%

- artificial sources (Anthropogenic / city light) ~ 9%



# Results examples

## Night time measurement of the UV background by EUSO-Balloon

**Author(s):** MACKOVJAK, Simon<sup>1</sup>

**Co-author(s):** NERONOV, Andrii<sup>1</sup>; MORETTO, Camille<sup>2</sup>; BACHOLLE, Simon<sup>3</sup>; BOBÍK, Pavol<sup>4</sup>; PUTIŠ, Marian<sup>4</sup>; DEL PERAL, Luis<sup>5</sup>; RODRIGUEZ FRIAS, Maria<sup>5</sup>; SHINOZAKI, Kenji<sup>6</sup>; CATALANO, Camille<sup>7</sup>; SORIANO, Jorge Fernández<sup>5</sup>; SÁEZ CANO, Guadalupe<sup>5</sup>

<sup>1</sup> ISDC - Data Centre for Astrophysics, Astronomy Department, University of Geneva, Switzerland

<sup>2</sup> Laboratoire de l'Accélérateur Linéaire, Université Paris Sud, France

<sup>3</sup> Laboratoire AstroParticule et Cosmologie, Université Paris Diderot, France

<sup>4</sup> Department of Space Physics, Institute of Experimental Physics, Slovak Academy of Science, Slovakia

<sup>5</sup> Space and Astroparticle Group, University of Alcalá, Spain

<sup>6</sup> Institute for Astronomy and Astrophysics, University of Tübingen, Germany

<sup>7</sup> Institut de Recherche en Astrophysique et Planétologie, CNRS-UPS Toulouse, France

**Corresponding Author(s):** [simon.mackovjak@gmail.com](mailto:simon.mackovjak@gmail.com)

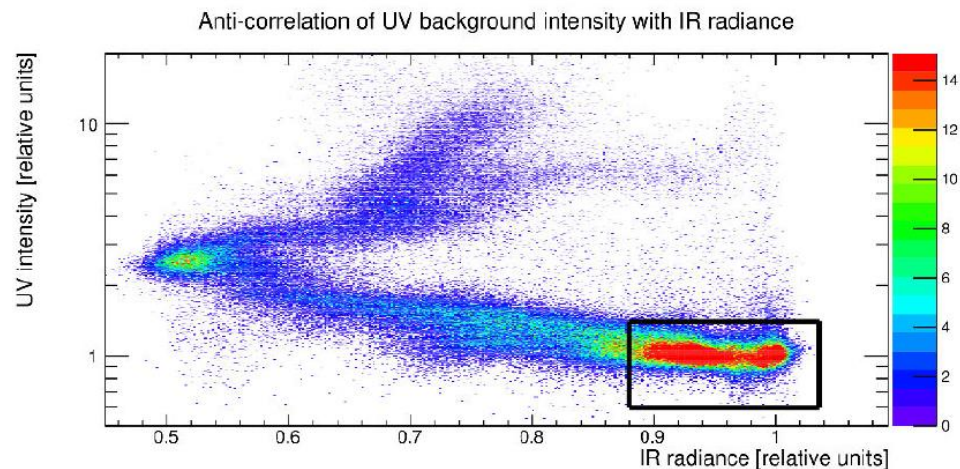
Precise characterization of the Earth night side UV background is essential for observation of the ultra-high-energy cosmic ray induced extensive air showers (EAS) from the space. We have analyzed data from the flight of EUSO-Balloon pathfinder mission that took place near Timmins (Canada) in the moonless night from 24<sup>th</sup> to 25<sup>th</sup> August 2014. The EUSO-balloon telescope imaged the UV background in the wavelength range 290–430 nm from the altitude ~38 km with a 1 m<sup>2</sup> refractor telescope with 11.5° field-of-view pointed in nadir direction. The UV data were complemented by the data of the Infrared (IR) camera onboard EUSO-balloon, which operated in the wavelength ranges 10.37–11.22  $\mu$ m and 11.57–12.42  $\mu$ m. We have combined the UV and IR images to study the upward UV radiance from the Earth surface and Earth atmosphere. This allowed us to estimate UV background in clear atmosphere conditions without man-made lights and also to investigate influence of clouds on the UV background values. The obtained UV intensity for clear atmosphere conditions is in a good agreement with previous BaBy and NIGHTGLOW balloon measurements. Comparison of the UV and IR images reveals a strong dependence of the upward UV radiance on the atmospheric conditions, so we discuss the possibility to use the UV albedo effect for characterization of the clouds. For estimating the observation efficiency of EAS from space by EUSO like detectors, it is important to determine the time variation of average UV background intensity, cloud distribution and local man-made light. Using available data, we also discuss these key factors that determine the observable time and area for EAS observation.

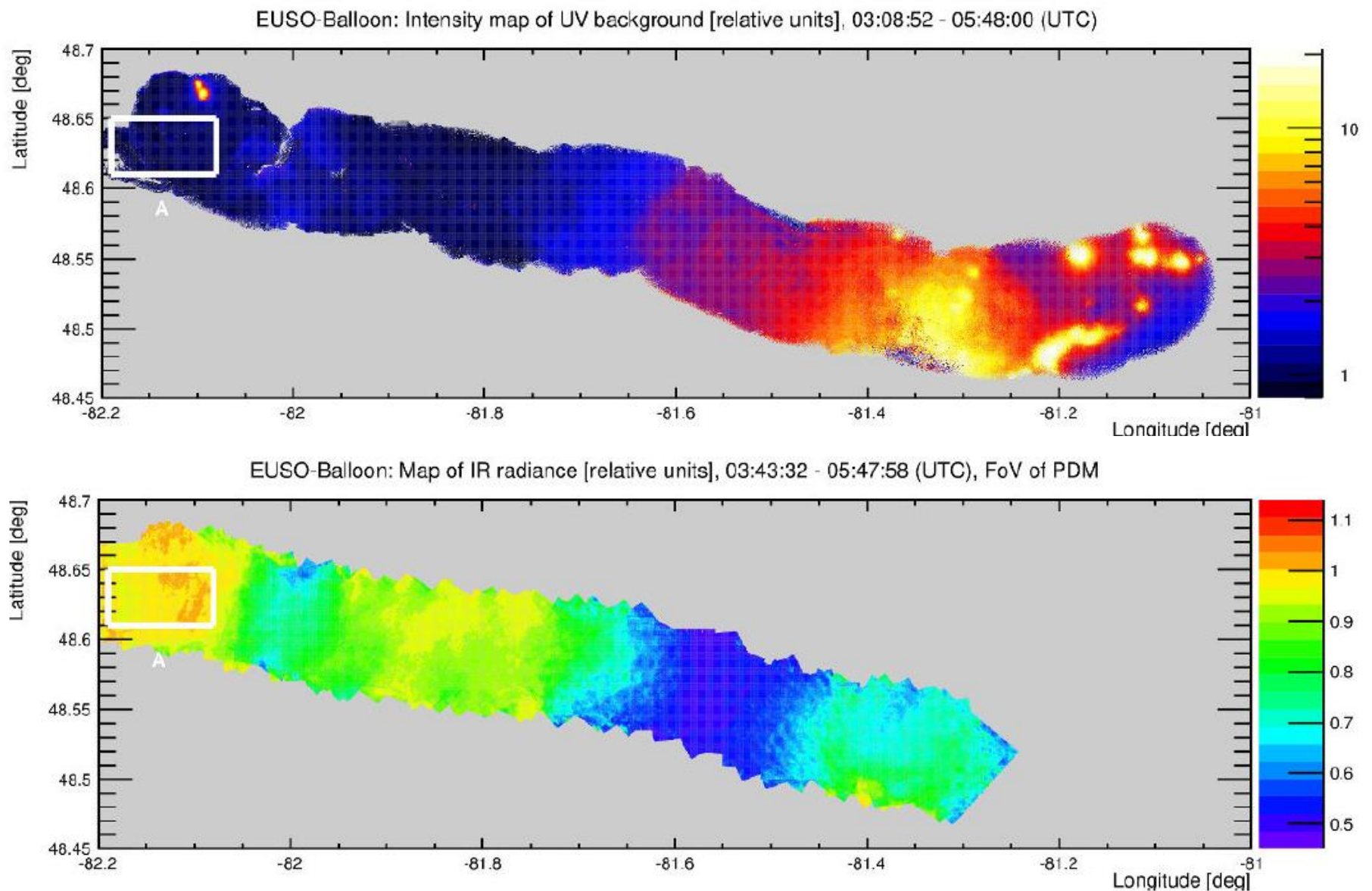
## Main results

- EUSO-Balloon is the first mission that imaged the UV background in different atmospheric conditions, well monitored by dedicated Infrared Camera

- An anti-correlation between UV and IR up-going radiation was found and an evident dependence of the UV background on atmospheric conditions was revealed

- The tool for masking the regions affected by clouds and manmade light in the FoV is prepared to fulfill the requirements for a high quality detection of UHECR

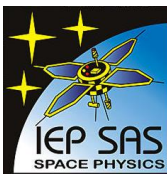




- The displayed values are relative to the mean value of  $I_{BG}$  over reference area "A" (white box)
- Pixels with the lowest IBG and the highest IR radiance correspond to clear atmosphere
- The clouds have higher albedo than ground and increased IBG values
- The pixels affected by man-made lights (the city Timmins with neighborhoods, mines, and airport) do not follow the general IR-UV anti-correlation



# Results examples



## Pattern recognition study for different levels of UV background in JEM-EUSO experiment

**Author(s):** PASTIRČÁK, Blahoslav<sup>1</sup>

**Co-author(s):** BOBÍK, Pavol<sup>1</sup> ; PUTIŠ, Marián<sup>1</sup> ; VRÁBEL, Michal<sup>2</sup> ; VASILKO, Ján<sup>3</sup> ; BERTAINA, Mario<sup>4</sup> ; SHINOZAKI, Kenji<sup>5</sup> ; FENU, Francesco<sup>6</sup>

<sup>1</sup> *Institute of Experimental Physics SAS, Košice, Slovakia*

<sup>2</sup> *Technical University Košice, Slovakia*

<sup>3</sup> *Technical University Košice Slovakia*

<sup>4</sup> *Univ. & INFN Torino*

<sup>5</sup> *Institute of Astronomy and Astrophysics, Universitat Tübingen, Tübingen, Germany*

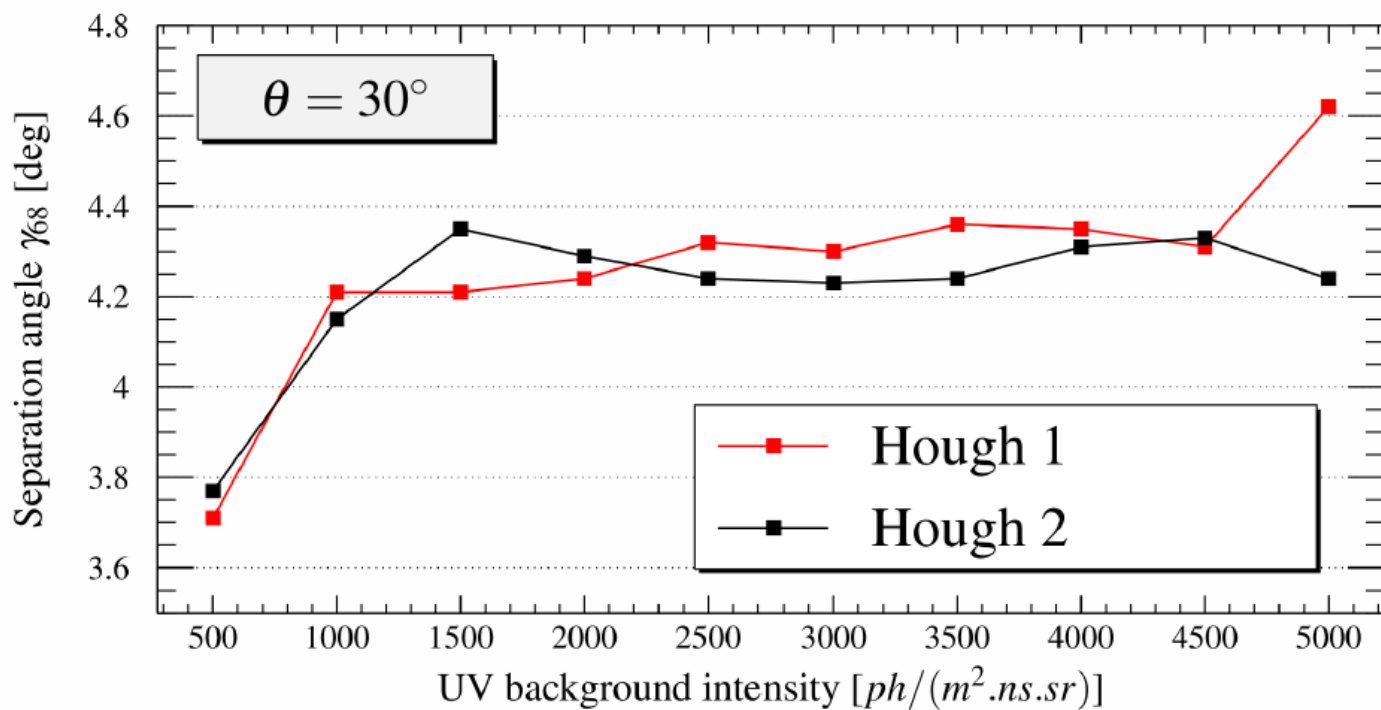
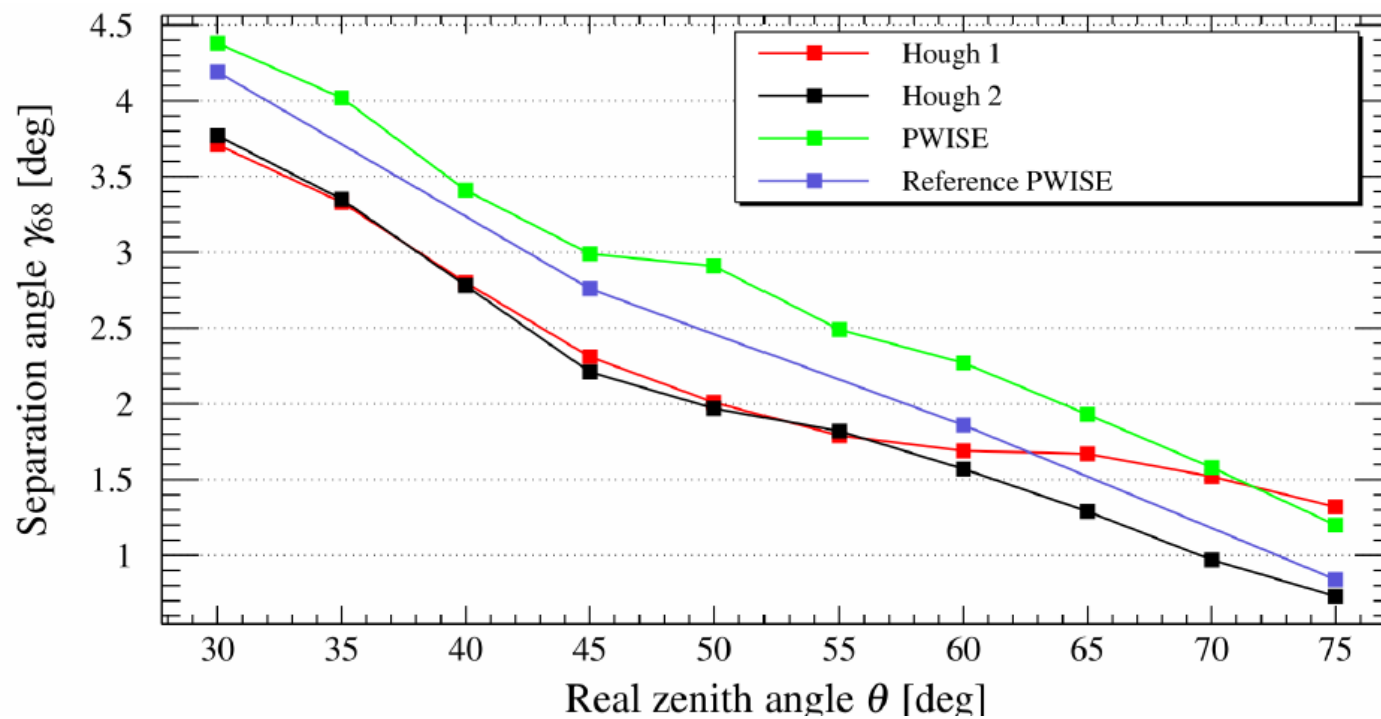
<sup>6</sup> *Department of General Physics, University of Torino, Torino, Italy*

**Corresponding Author(s):** slavo@saske.sk

JEM-EUSO experiment will observe UV light created by extensive air showers initiated by ultra high energy cosmic rays (UHECR). Reconstruction of UHECR particle direction from detected signal depends also on the level of signal background, which can vary in time and with location.

We developed an alternative pattern recognition (PR) method based on Hough transformation besides to existing PR methods in JEM-EUSO software framework. The results of them, namely of PWISE method and Hough method were compared for the nominal UV background 500 ph/(m<sup>2</sup> ns sr). Hough method was used to evaluate UHECR direction reconstruction ability for higher level of the UV backgrounds on the Earth's night side. The study what impact on fake trigger events rate come from varying background levels was performed, too.



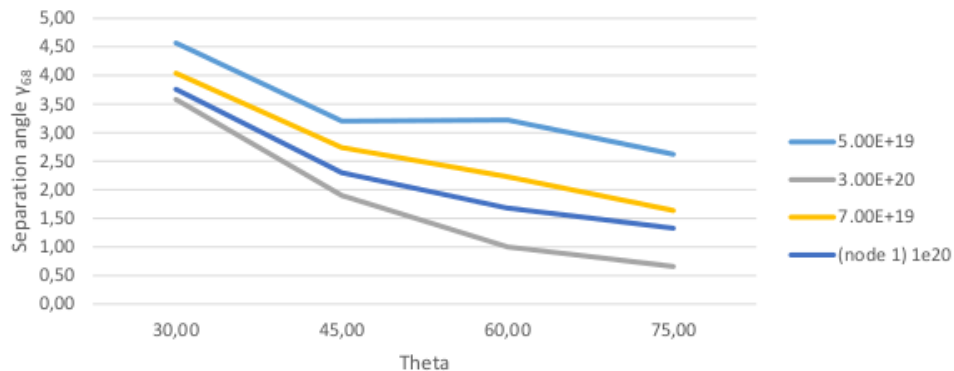


# Results examples

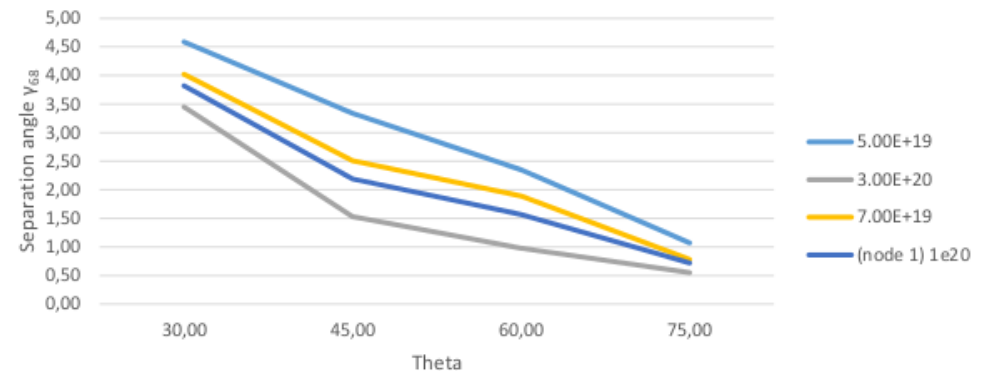
## Precision of angular reconstruction (1)

energy of primary particle ... eV ; background **500** ph/(m<sup>2</sup> ns sr)

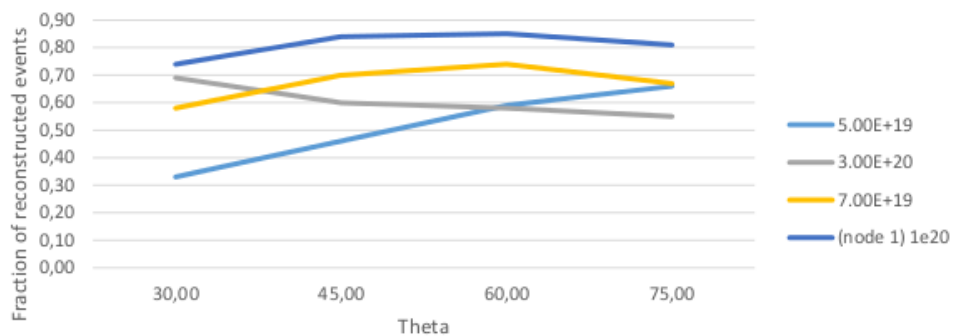
Hough 1 - Best  $\gamma_{68}$  (rmax=inf)



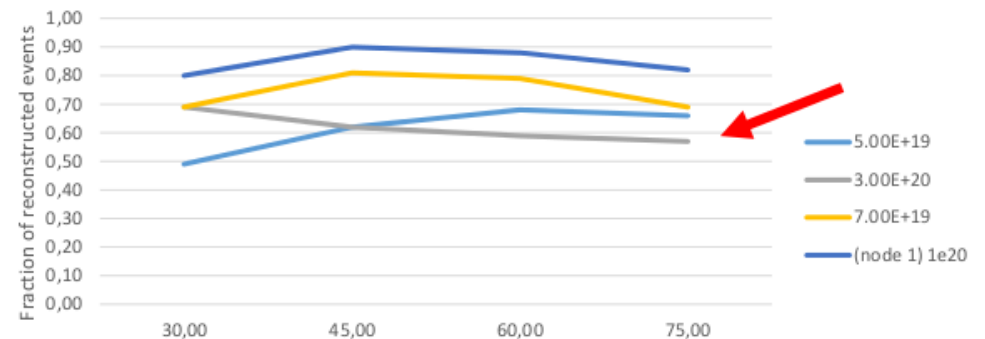
Hough 2 - Best  $\gamma_{68}$  (rmax=inf)



Hough 1 - Best  $\gamma_{68}$  : fraction of reconstructed events (rmax=inf)



Hough 2 - Best  $\gamma_{68}$  : fraction of reconstructed events (rmax=inf)



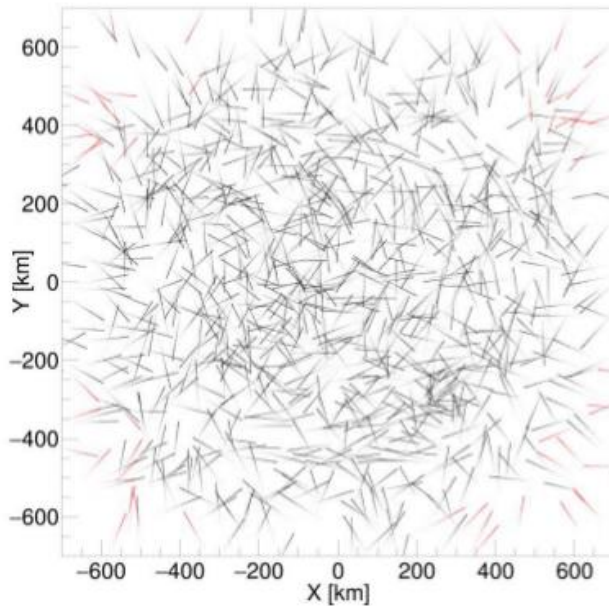
# Results examples

## Precision of angular reconstruction (3)

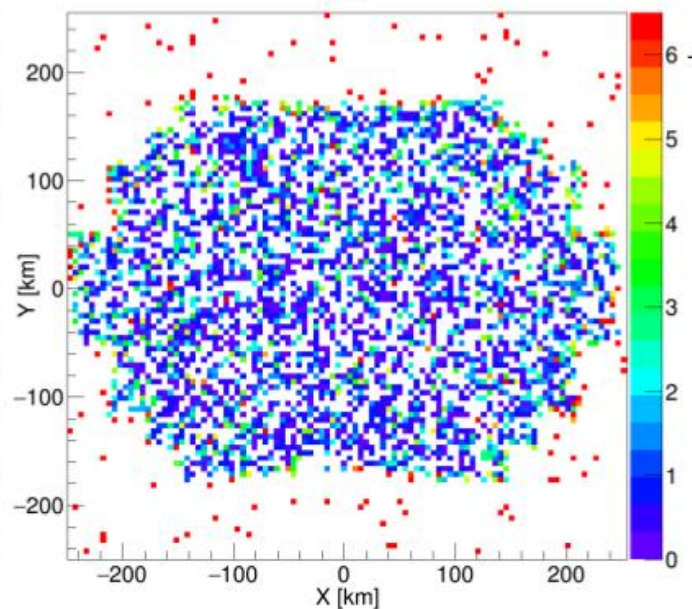
energy of primary particle ... eV ; background **500** ph/(m<sup>2</sup> ns sr)

$\gamma$  vs. position of shower maximum

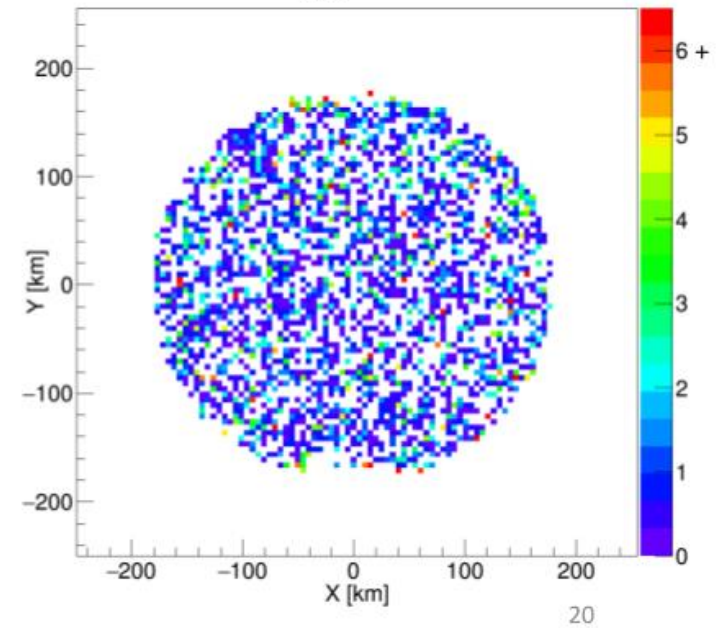
Simulated showers



$r_{\max} = \text{inf}$



$r_{\max} = 180$  km



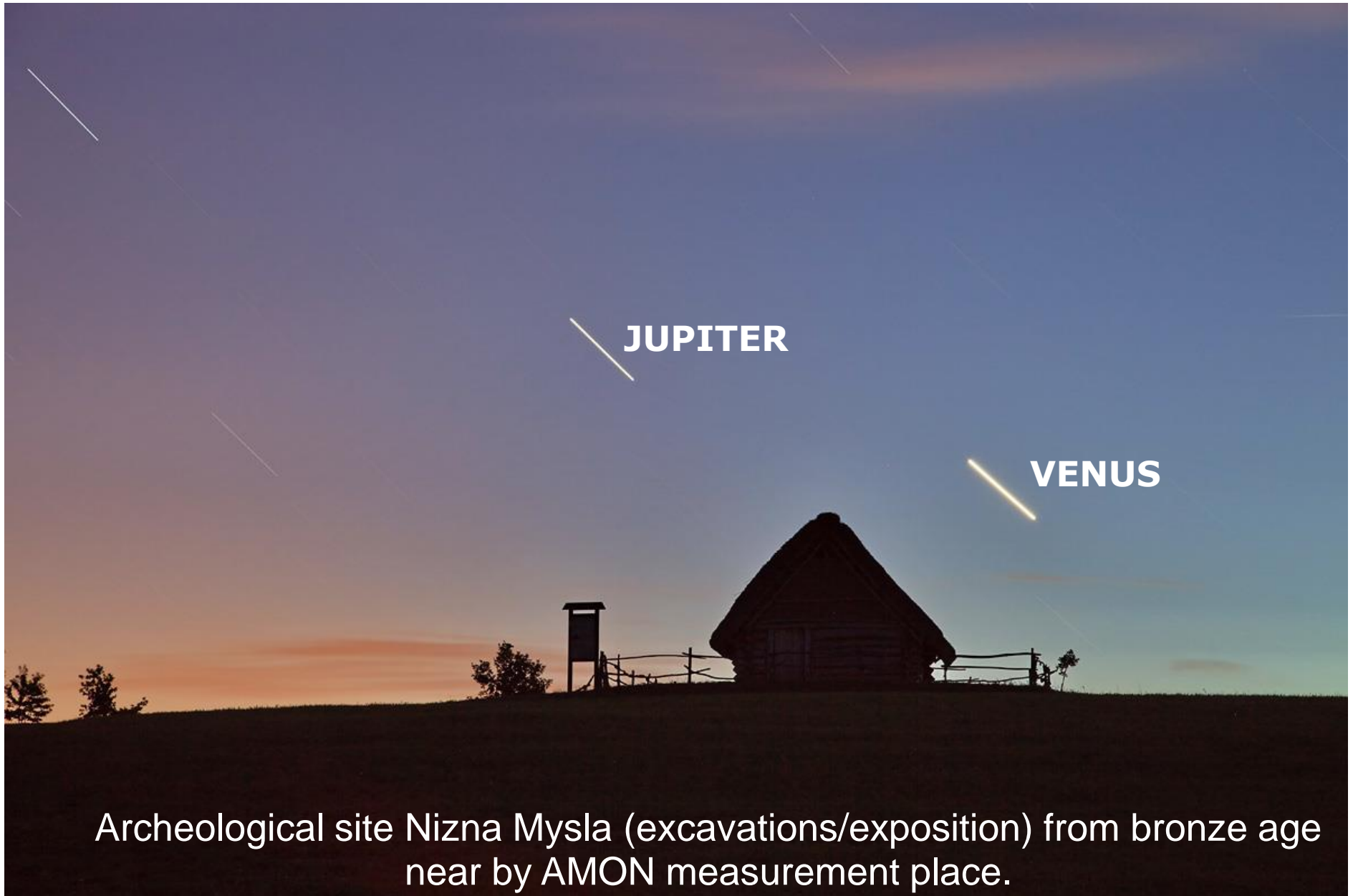


# AMON, **A**irglow **MON**itor



- . One pixe UV background detector
- . DAQ 50 bits/second, 1 second integration
- . Small & cheap, appropriate to measure BG
- . Optical sensor: actually Hamamatsu microPMT, could be another one, for example M1
- . BG3 filter, easy to change another filters
- . Collimator: FoV, in order of 1 degree
- . No optics
- . Power consumption:  $< 0.5W$  ( $< 0.05W$  stand by)
- . Dimmensions: 110x75x60mm
- . Weight: 0.58 kg

# First test measurements 17.-18. june 2015



Archeological site Nizna Mysla (excavations/exposition) from bronze age  
near by AMON measurement place.

# Current version of AMON detector





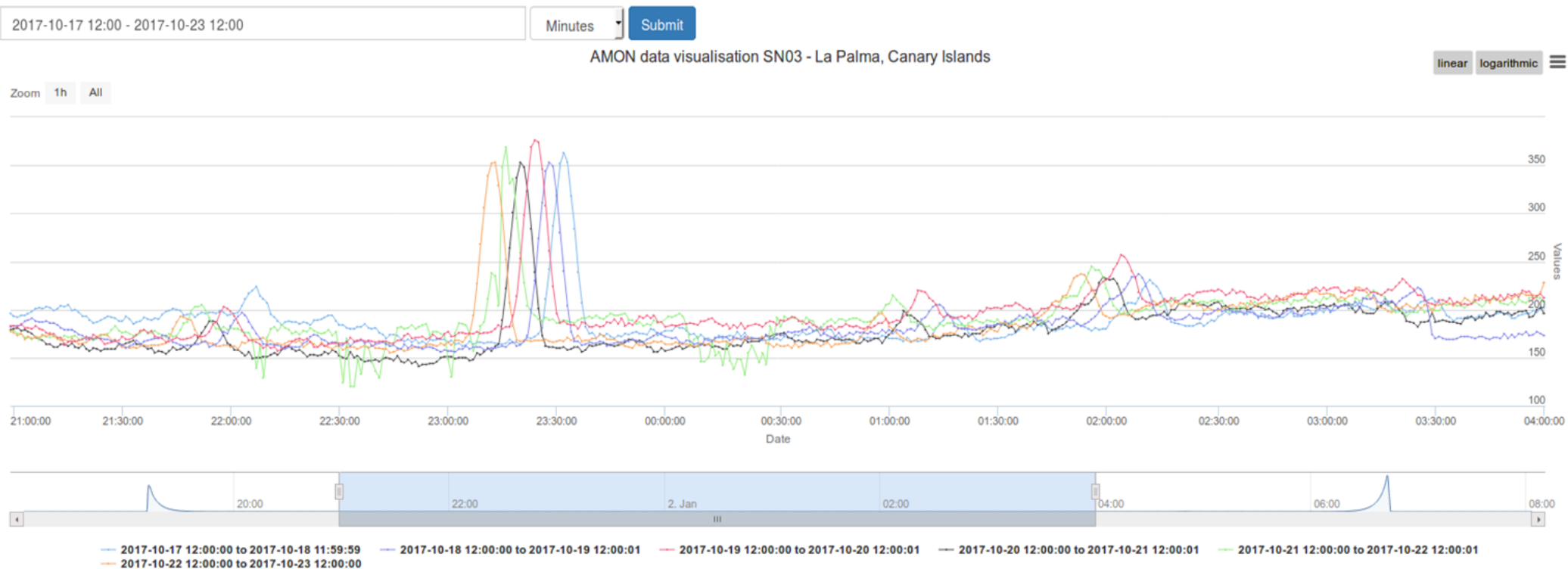


# AMON-net

## - Airglow **MON**itor **net**work :

- four stations
- Lomnický štít, Slovakia (soon Kolonica)
- Observatorio del Roque de Los Muchachos, La Palma, Spain
- Observatorio Astronomico Nacional de San Pedro Martir, Mexico
- Stockholm, Sweden

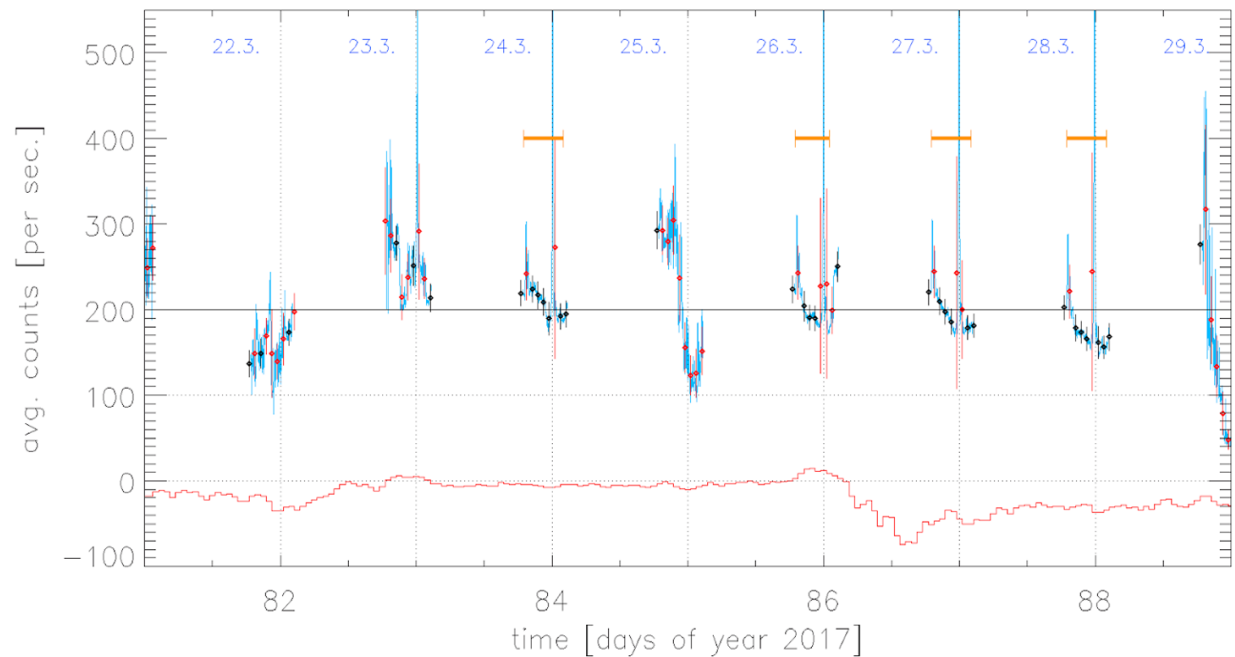
ORM, La Palma, Spain





# AMON-net

- **main observational tasks**
- dynamics of airglow
- response of airglow production to geomagnetic disturbances
- night variations
- seasonal variation
- geographical variation
- atmospheric gravity waves



The example of AMON measurements at Lomnický štít in 2017. The blue line represents data (a measured intensities) with one minute step. The black and red diamonds represent a one hour data. The lines over and under hours points show standard deviation. Red are those with non Poissonian distribution, black are those with Poissonian distribution. The red points were excluded from the analysis.



**Thank you**



## ESA PECS: SK1\_05

AO/1-8224/15/NL/NDe - 1st Call under PECS in Slovakia

From 1.june 2016 to 30.4.2018

The objective of the proposed project is a study of night-time UV background models and data for the estimation of ionospheric disturbances visibility, especially during active years of the solar cycle, in night-time UV airglow light that is produced by upper atmosphere of the Earth. We will analyze if the available UV background models and data could be compared with the measurements of relatively simple and inexpensive ground-based one pixel UV detector. Feasibility study of ionospheric disturbances observation by one pixel detector is the main objective of this proposal.

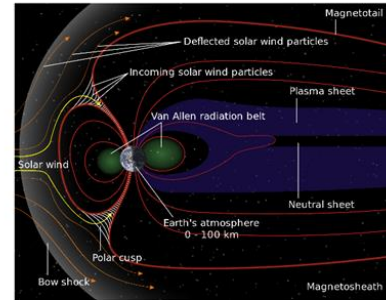
Budget: 50 kEUR

**BACK-UP SLIDE**

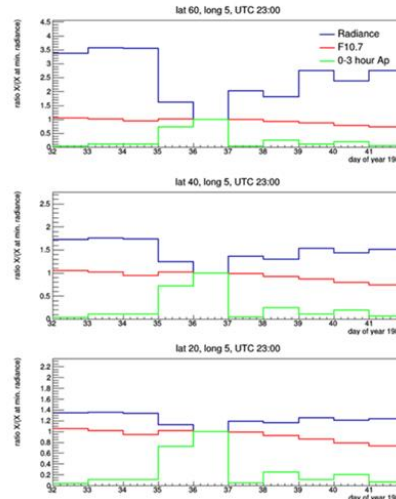
The objective of the proposed project is a study of night-time UV background models and data for the estimation of ionospheric disturbances visibility, especially during active years of the solar cycle, in night-time UV airglow light that is produced by upper atmosphere of the Earth. We will analyze if the available UV background models and data could be compared with the measurements of relatively simple and inexpensive ground-based one pixel UV detector. Feasibility study of ionospheric disturbances observation by one pixel detector is the main objective of this proposal.



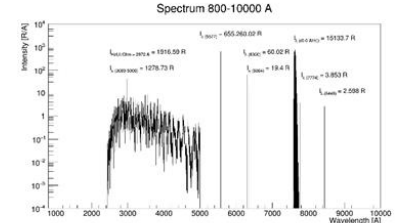
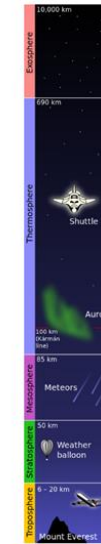
Airglow layer. Credit: NASA



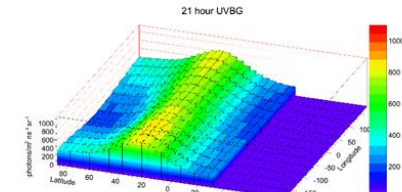
Interaction between Sun and Earth's atmosphere is responsible for airglow radiation of upper atmosphere.



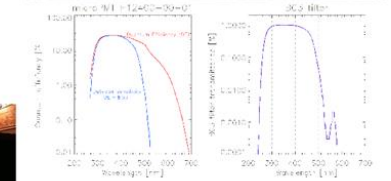
Upper atmosphere light production (blue line), Ap 3 hours index (green line) and F10.7 index (red line) evolution in 10 days time window starting 4 days before storm maximum (i.e. in undisturbed period). Storm with maximum at 4. - 5. february 1983.



Nightglow radiation in range from 200 to 500 nm is produced by photodissociation of  $O_2$  and consequent combination of atomic oxygen followed by photon emission.



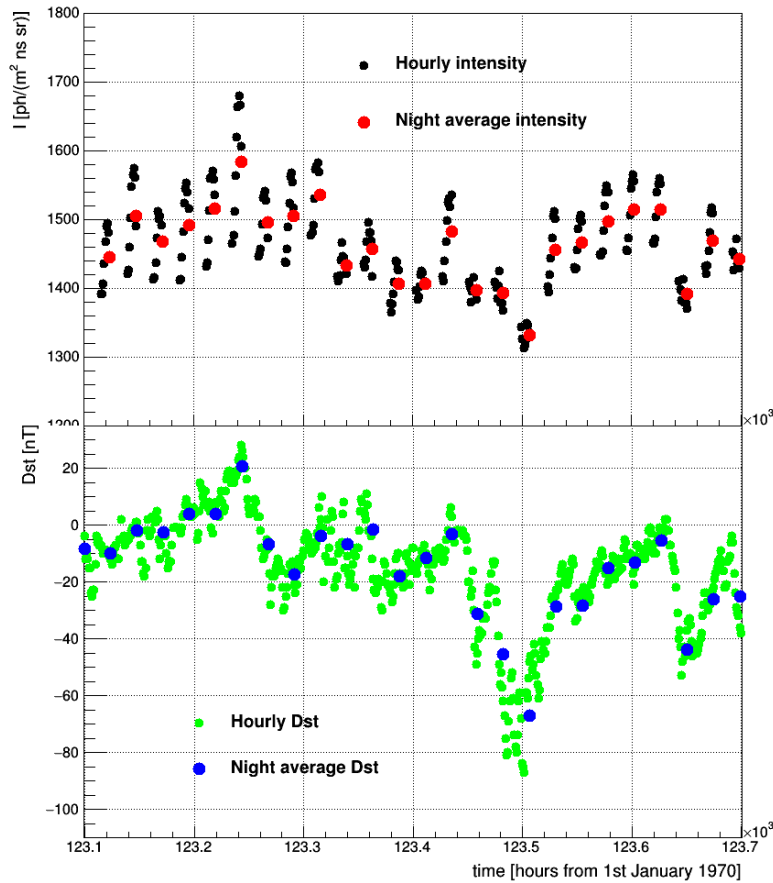
Airglow production distribution over the Earth, example. Same local time, 21:00, december 1994.



One pixel UV detector, response, quantum efficiency and transmittance of optical filter.

Measurements of the variability of airglow light produced in lower ionosphere can provide additional information on ionospheric disturbances to existing and proposed experiments based on different physical principles. To our knowledge there is no complex study of this topic in UV spectral range. Furthermore such study could be important for detection of extensive air showers induced by ultra high energy cosmic rays with fluorescence telescopes from the Earth orbit.

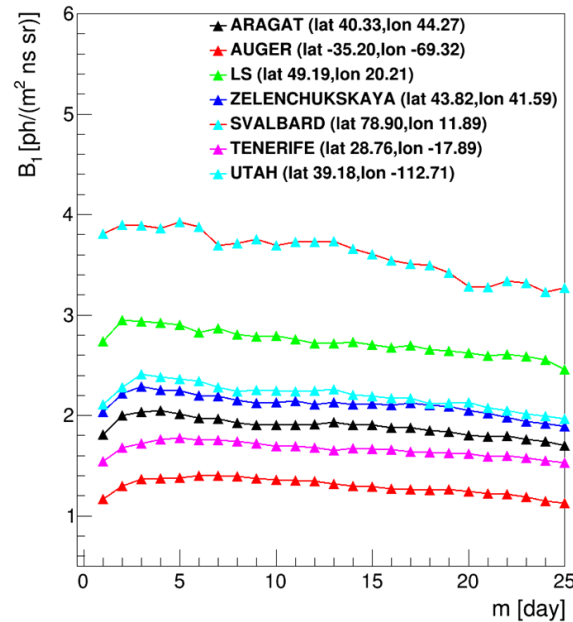
LS (lat 49.19,lon 20.21)



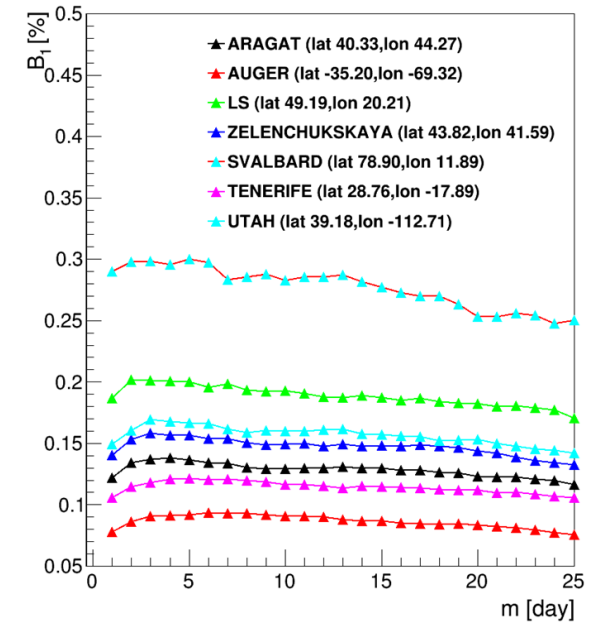
# Project summary / Work package 3

from 01/12/2016 to 31/05/2017

Selected stations, fit parameter  $B_1$  for  $\Delta I$  [ph/(m<sup>2</sup> ns sr)]



Selected stations, fit parameter  $B_1$  for relative  $I$  [%]



Time series of airglow production (top) and Dst index time evolution (bottom) for Lomnický štít position.

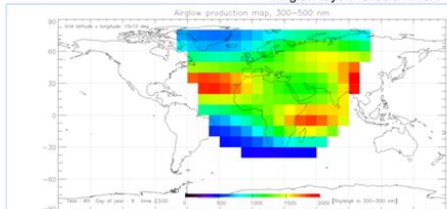
$B_1$  parameter as a function of preceding period length  $m$  for seven selected geographical positions.



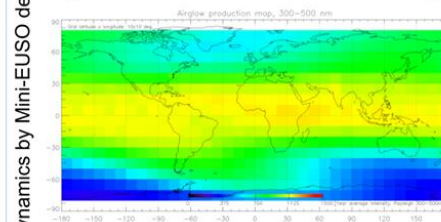
Mini-EUSO ("UV atmosphere" in Russian Space Program) will observe Earth night side atmosphere from ISS in the UV band. The observed light consists mainly of light produced by airglow. We investigate the feasibility to observe airglow dynamics by Mini-EUSO detector. The investigation focuses on observability of two effects. One is the observability of magnetic storms in airglow light, where we expect decreasing light production in UV during storms. The other is the possibility to detect patterns created by atmospheric gravity waves induced by tsunami waves.



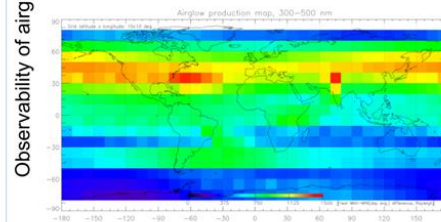
Airglow layer. Credit: NASA



Airglow production at 9 January, 1980, 23:00 UT, in the wavelength range 300 - 500 nm.

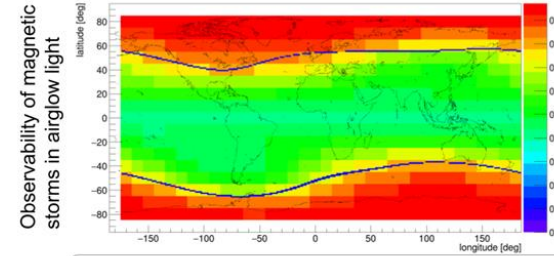


Annual average of airglow light production for year 1980



Seasonal variation of airglow light production in the year 1980

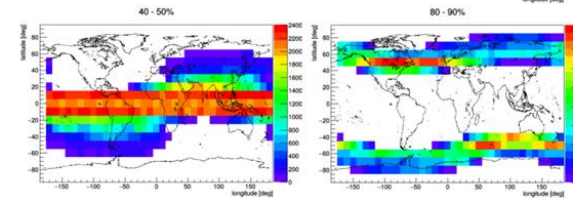
Observability of airglow dynamics by Mini-EUSO detector



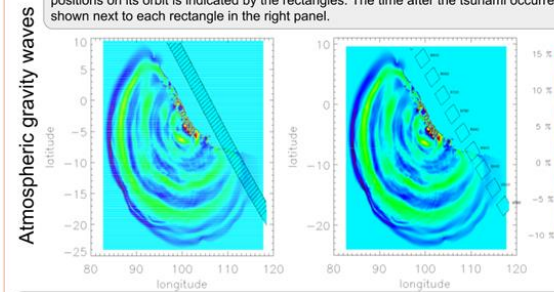
Average relative deviation between  $A_p = 0$  and  $A_p = 250$  during period between 1970 and 1994. Borders of auroral oval at  $K_p = 8$  are represented by blue line.

Airglow sensitivity to magnetospheric disturbances. Relative deviations ( $A_p = 0$  vs  $A_p = 250$ ) for all geographical grid positions. For given interval, histograms show number of occurrences for each position at map. Relative deviations are for period between 1970 and 1994.

$$\text{Average relative deviation} = \frac{1}{N} \sum_{i=1}^N \frac{|I_{A_p=0} - I_{A_p=250}|}{I_{A_p=0}}$$



Example of Mini-EUSO flight over the tsunami. The Mini-EUSO FoV for the different positions on its orbit is indicated by the rectangles. The time after the tsunami occurrence is shown next to each rectangle in the right panel.



The results from analysis preliminary indicate, that Mini-EUSO could register tsunami waves in observed airglow light during the cloudless observations/conditions. The influence of effects hampering a waves observations as clouds in FoV will be tested in further analysis.

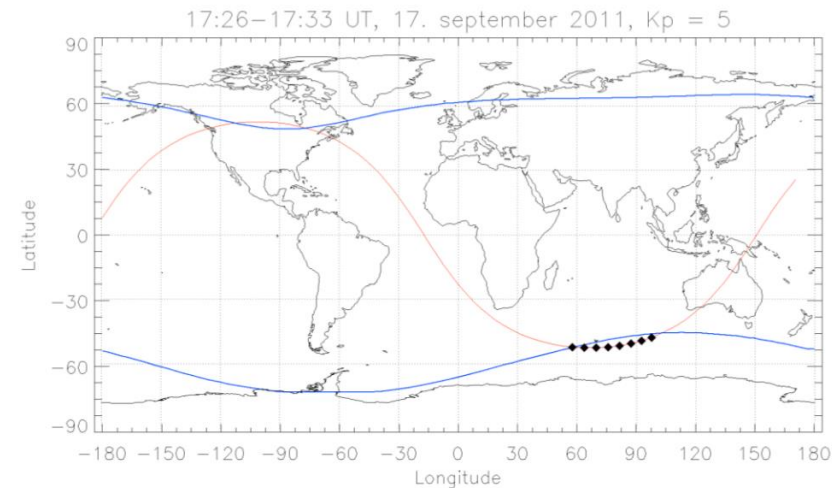
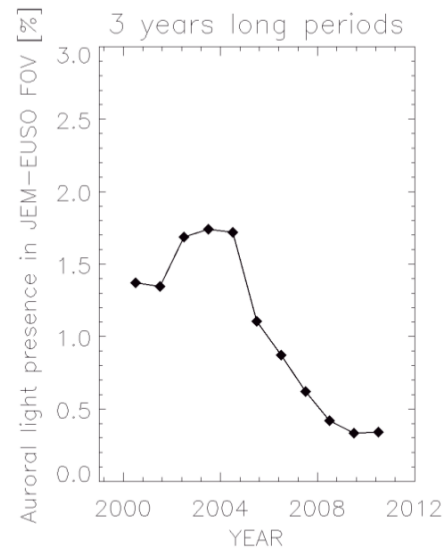
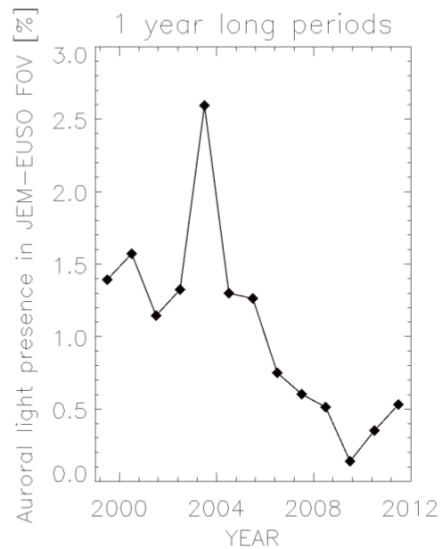
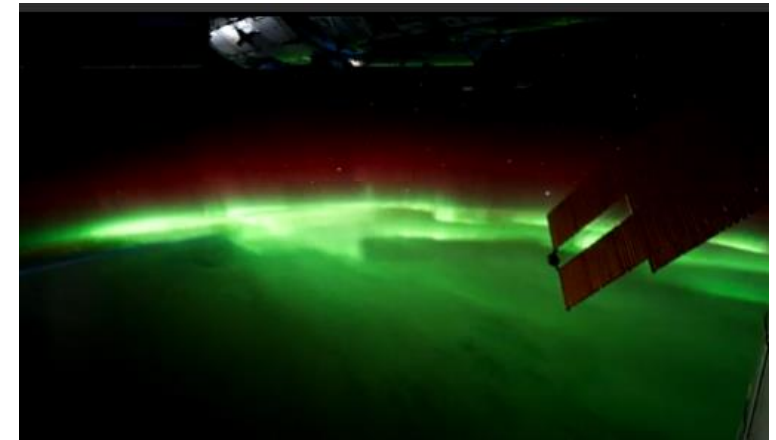
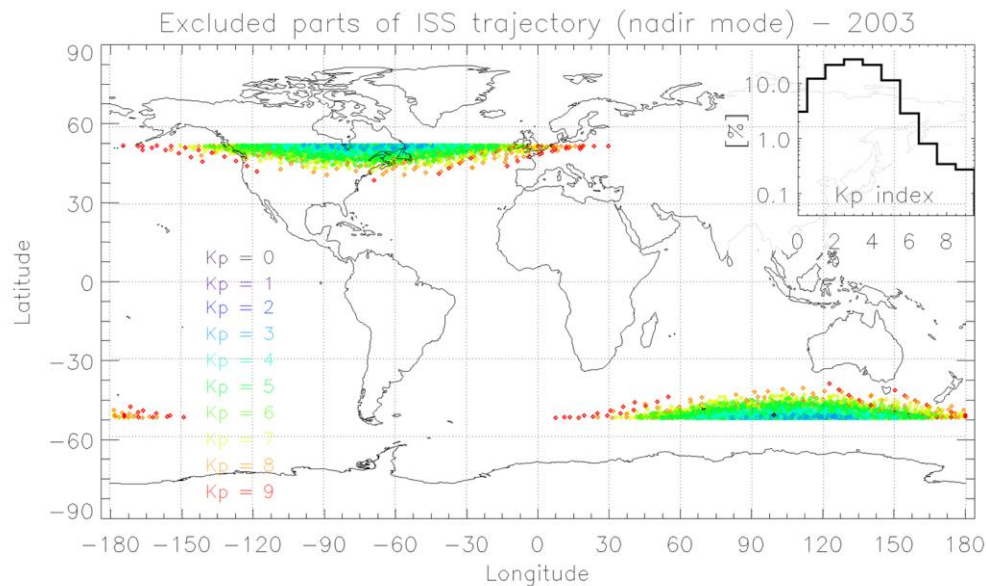
**Conclusion:** Mini-EUSO at ISS will offer interesting possibility to observe UV airglow. Relatively long Mini-EUSO operation time (hundreds of days) allow production of geographical and time dependent maps of UV upward radiation which include as most dynamic part airglow. These data bring insight to seasonal and geographical variation of airglow in ISS orbit area. Airglow depends also on geomagnetic field. Effect of changes in geomagnetic parameters during geomagnetic disturbances will be investigated in Mini-EUSO data. We expect decrease in airglow light level during such events.

**Acknowledgment:** This work was partially supported by State Space Corporation ROSCOSMOS, as well as by Slovak Academy of Sciences MVTS JEM-EUSO, VEGA grant agency project 2/0132/17, ASI contract 2016-1-U.O "MINI-EUSO" as well as by the government of Slovakia through an ESA contract under the PECS (Plan for European Cooperating States). ESA disclaimer: The view expressed herein can in no way be taken to reflect the official opinion of the European Space Agency.



# Duty cycle estimation

## Auroras effect on JEM-EUSO operational efficiency



Advances in Space Research article

Figure 3: Left panel: Fraction of time  $f_{AL}$  in which auroral light restrain EAS measurements for one year long periods from 2000 to 2011. Right panel: Same as in the left panel, but integrating for 3-year periods.

**BACK-UP SLIDE**